DETERMINING LONG-TERM DENUDATION RATES, USING *IN SITU*-PRODUCED ^{10}BE COSMOGENIC NUCLIDES

by

HOLDEN D. ARONSON

(Under the Direction of Paul Schroeder)

ABSTRACT

Land management practices can be improved upon by elucidating the ways in which human activity can drastically change denudation rates. Severe erosion is exacerbated in the southern Appalachian Piedmont region of the United States where native forest was cleared for farming and tilling in the early 18th century, undergoing no conservation until the mid-20th century. The use of ^{10}Be cosmogenic nuclide dating quantifies the amount of time sediment has been exposed to cosmic rays; thus by utilizing *in situ*-produced ^{10}Be cosmogenic nuclides collected in fluvial sediments from Holcombe's Branch and Tyger River, millennial-scale denudation rate were measured (7.1 ± 0.2 m/Ma, n=7). Post-settlement hillslope erosion rates and sediment yield data in the southern Piedmont and Broad River Basin reflect elevated rates of erosion when compared to ^{10}Be derived denudation rates. Landscape management tactics can be aided by knowledge of the background (10,000-100,000 years ago) denudation rates to improve conservation measures.

INDEX WORDS: southern Appalachian Piedmont, ^{10}Be cosmogenic nuclides, denudation rate, erosion rate

DETERMINING LONG-TERM DENUDATION RATES, USING *IN SITU*-PRODUCED ^{10}BE COSMOGENIC NUCLIDES

by

HOLDEN D. ARONSON

B.S., Appalachian State University, 2021

A Thesis submitted to the Graduate Faculty of The University of Georgia in Partial Fulfillment of the Requirements for the Degree

MASTER OF SCIENCE

ATHENS, GEORGIA

2023

DETERMINING LONG-TERM DENUDATION RATES, USING *IN SITU*-PRODUCED ^{10}BE COSMOGENIC NUCLIDES

by

HOLDEN D. ARONSON

Major Professor: Paul Schroeder

Committee: Andy Darling
David Leigh

Electronic Version Approved:

Ron Walcott
Vice Provost for Graduate Education and Dean of the Graduate School
The University of Georgia
May 2023

DEDICATION

This research is dedicated to my late brother, Logan Aronson, who has meant and continues to mean so much to me. Although he is no longer here, nor had the opportunity for this adventure, his memories carry on and continue to regulate my life. You would have been so proud.

ACKNOWLEDGMENTS

I sincerely thank Dr. Paul Schroeder for his support and navigation throughout my time at the University of Georgia. Time and again you have assisted me to accomplish the goals I have longed for. Thank you to Andy Darling and David Leigh for your continued support and position on my committee.

Thank you to Paul Bierman and Lee Corbett for all your help and guidance while at the University of Vermont's Cosmogenic Laboratory. The five weeks I spent learning in your lab and exploring Burlington, Vermont was an amazing experience.

Thank you, Carla Hadden and Tom Maddox, for all you have done for me at the Center For Applied Isotope Studies. Tom, you have been an amazing supervisor the past two years. I could not have asked for a better supervisor.

A huge thank you to my geology graduate peers; Marjean Cone, Alexandra Bonham, Lea Davidson, Oluwaseun Adeyemi, Fabian Zowam, and all of my peers in the program for your help the past two years.

I would also like to thank a handful of people that have helped me get to this chapter in my life. Debra, Ron, Bryce, Logan, Peyton and Langdon Aronson, you have always been so supportive of me, constantly pushing me to reach the next level. Omid Bonakdar and George Sharpe, we have bounced motivation between each other for years now and you two have truly helped me get through the rough. This research was supported by the Nation Science Foundation and Miriam Watts-Wheeler Fund from the University of Georgia.

TABLE OF CONTENTS

Page

LIST OF TABLES

Page

LIST OF FIGURES

Page

CHAPTER 1

INTRODUCTION AND LITERATURE REVIEW

This thesis is organized into three chapters. Chapter one explains the overall background of this study. Chapter two comprises of an introduction, background, geologic setting, methods, results, discussion, and conclusions. The third chapter describes ideas for future research.

The purpose of this study was to quantify long-term denudation rates within the southern Appalachian Piedmont region of the United States. Over the past 300 years, human activity has drastically reshaped earth's surface. It is significant to understand how human activity alters the morphology of the landscape, so that land management tactics can improve (Reusser et al., 2015). The United States Soil Conservation Service, in the 1940's, found that the southern Appalachian Piedmont lost 18 cm of soil due to non-indigenous immigrant settling in the region (Reusser et al., 2015). In an area such as the Calhoun Critical Zone Observatory experimental forest, where intense farming and tilling occurred dating back to the early 18th century through the mid 20th century, extreme gulling and sediment polluted tributaries dominated. Short-term denudation rates calculated from the Watershed Erosion Prediction Project (WEPP) online program and previously published data measured in tributaries in North Carolina, South Carolina, and major global rivers exemplify how the landscape is eroding after the arrival of non-indigenous immigrants (Simmons, 1993; Summerfield and Hulton, 1994; Trimble, 1977; Wilkinson and McElroy, 2007). Due to rare/extreme weather events and sediment traps and dams, the sediment yield data is difficult to interpret long-term anthropogenic effects in heavily cultivated areas, compared to newer methods (Granger, 1996). This study uses *in situ*-produced

^{26}Al and ^{10}Be cosmogenic nuclide isotopes, collected in quartz grains from tributaries and soil profiles within the Calhoun Critical Zone Observatory, to better understand the average basin-wide natural or background (10,000 – 100,000 years ago) denudation rate, before the arrival of non-indigenous immigrants (Reusser et al., 2015).

In the past 25 years, cosmogenic nuclide dating has become increasingly popularized (Granger, 2013). Ten major basins in the southern Appalachian Piedmont, stretching from Virginia to Alabama, have previously been studied for sediment yield and *in situ*-produced ^{10}Be cosmogenic nuclides to quantify long-term denudation rates, except for the Broad River Basin (Reusser et al., 2015; Trimble, 1977). It is difficult to determine the background rates of erosion based on short-term methods such as sediment flux rates (Trimble, 1974; 1977; Granger, 1996). By using fluvial quartz grains that have been homogenized through hillslope processes and bioturbation an average basin-wide denudation rate can be determined (Bierman and Steig., 1996; Brown et al., 1995; Granger et al., 1996; Reusser et al., 2015)

Non-indigenous immigrants, through intense farming practices, accelerated the rate at which soil erodes on interfluves in the Calhoun Critical Zone Observatory (Coughlan and Nelson, 2018). By the late 20th century, a study found that ~1 m of legacy sediments, sediment transported due to anthropogenic influence, accumulated in the Holcombe's Branch stream, valley bottoms, and toe slopes dating back to the beginning of the 19th century (Wade et al., 2020). This research uses fluvial sediments collected in Holcombe's Branch and Tyger River, sub watersheds to the Broad River Basin, and soil pits in adjacent sub watersheds to measure the cosmogenic concentrations on hillslope transported quartz grains and at depth horizons (Bierman and Steig., 1996; Brown et al., 1995; Granger et al., 1996; Reusser et al., 2015; Schroeder et al., 2022). Determining the background denudation rate to compare to post non-indigenous

immigration and post soil conservation is significant in understanding how human activity can shape landscape features, further aiding to improve soil conservation measures (Reusser et al., 2015).

CHAPTER 2

DETERMINING LONG-TERM DENUDATION RATES, USING *IN SITU*-PRODUCED ^{10}BE COSMOGENIC NUCLIDES

Aronson, Holden. To be submitted to the *Journal of Sedimentary Research*

Abstract

Land management practices can be improved upon by elucidating the ways in which human activity can drastically change erosion rates. Severe erosion is exacerbated in the southern Appalachian Piedmont region of the United States where native forest was cleared for farming and tilling in the early 18th century, undergoing no conservation until the mid-20th century. The use of ^{10}Be cosmogenic nuclide dating quantifies the amount of time sediment has been exposed to cosmic rays; thus by utilizing *in situ*-produced ^{10}Be cosmogenic nuclides collected in fluvial sediments from Holcombe's Branch and Tyger River, millennial-scale denudation rates were measured (7.1 ± 0.2 m/Ma). Post non-indigenous immigrant settlement, hillslope erosion rates and sediment yield data in the southern Piedmont and Broad River Basin reflect elevated rates of erosion when compared to ^{10}Be derived denudation rates. Landscape management tactics can be aided by knowledge of the background denudation rates to improve conservation measures.

Introduction

Knowing the rate that soil is produced and eroded is significant for understanding how landforms evolve over time (Heimsath et al., 2005; Wells and Andriamihaja, 1993; Willet and Brandon, 2002; Junger et al., 2009). An accurate background (long-term) denudation rate was not capable of interpretation by past methods, which is why a new approach to quantify rates of erosion has been developed (Reusser et al., 2015). This information is useful for making land management and agriculture recommendations, as well as understanding the forces that shape the earth's surface over long periods of geologic time (Heimsath et al., 2005; Jungers et al., 2009; Wells and Andriamihaja, 1993; Willet and Brandon, 2002; Richter et al., 2020).

Human activity, such as deforestation for timber harvest and agriculture, can drastically increase the sediment transported down a hillslope (Reusser et al., 2015, Trimble, 1977). This can be a result of the removal of vegetation that holds soil in place or the creation of new pathways for water to flow, leading to erosion and the movement of sediment (Hook, 1994; Reusser et al., 2015). If human-induced land disturbance leads to erosion rates that outpace the rate at which streams can access and transport the sediment to them, then sediment yield data represents neither natural erosion rates nor the maximum rate of upstream erosion (Reusser et al., 2015). Instead, the data may indicate how well the slopes are connected to channels, and in most cases, much of the sediment caused by human activities will stay trapped on hillslopes and valley bottoms (Haggett, 1961; Walling, 1983; Wilkinson and McElroy, 2007; Walter and Merrits, 2008; and Reusser et al,. 2015). In the past, short-term erosion rates in watersheds have been calculated using sediment yields to understand how soil is transported (Granger, 1996). While these calculations are useful, they do not show how the land is eroding on the millennial or geological time scale ($10^3 – 10^6$ years) in areas of high human activity, with the accuracy that cosmogenic dating does (Simmons, 1993; Summerfield and Hulton, 1994; Trimble, 1977). Sediment flux rates are prone to error due to sediment discharge during rare/extreme weather events, and sediment traps and dams (Granger, 1996). Comparing hillslope erosion with sediment yield data shows the inconsistency between the two during peak agricultural use in 1900, with a sediment delivery ratio of only 6% being transported to basin outlets (Trimble, 1977).

Over the past 25 years, cosmogenic nuclides have transformed the quantitative understanding of Earth's surface processes and evolution (Granger et al., 2013). Two ways cosmogenic nuclides can be measured is by *in-situ* produced and *meteoric* cosmogenic nuclides

(Granger et al., 2013). In this study, *in situ*-produced ^{10}Be and ^{26}Al cosmogenic nuclides are measured in fluvial and soil quartz grains. A key aspect of pairing ^{10}Be ($^{1}/_{2}$-life ~1.5 Ma) (Hofmann et al., 1987) and ^{26}Al ($^{1}/_{2}$-life ~0.7 Ma) (Norris et al., 1983) isotopes is due to its long half-life, as well having different half-lives to compare decay rates (Chmeleff et al., 2010; Nishiizumi, 2004). Cosmogenic nuclides are a recent technique in determining denudation rates by showing how long quartz grains have been exposed to cosmic rays near the surface (Granger, 1996). In the upper ~1 m of Earth's surface, ^{10}Be and ^{26}Al concentrations are homogenized as hillslope sediments are reworked by organisms and pedological processes, such as creep and tree-throw (Reusser et al., 2015). *In situ*-cosmogenic nuclides are produced in quartz grains by secondary cosmic radiation bombarding atomic nuclei (Granger, 2013). The longer a quartz grain has been exposed near the surface, the more cosmogenic isotopes will be produced (Granger, 2013). In this study, five samples were collected in Holcombe's Branch catchment and two samples were collected in the Tyger River for ^{10}Be cosmogenic analysis (Fig. 1). To get an average denudation rate of the Broad River Basin, ^{10}Be cosmogenic nuclides were measured in fluvial sediments (Granger, 1996). Modern river sediments withhold the ^{10}Be isotopic signature of long-term hillslope erosion (von Blackenburg et al., 2004). In a previous study, eleven pits were dug in the CCZO, proximal to Holcombe's Branch watershed, where soil samples were collected at depths ranging from 0 – 900 cm (Schroeder et al., 2022). To better understand denudation rates in the soil profiles around the CCZO, ^{10}Be and ^{26}Al cosmogenic concentrations were measured for a future study (Schroeder et al., 2022).

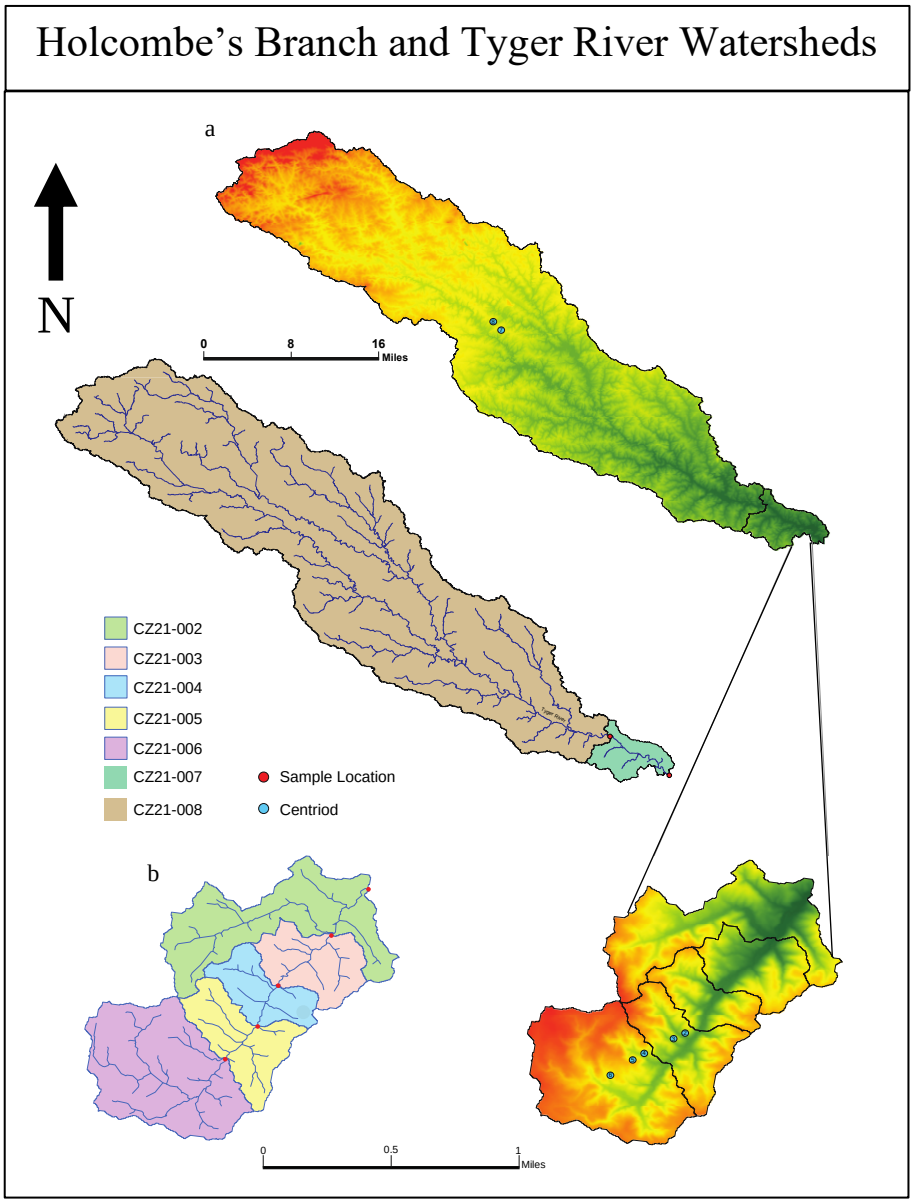

Fig. 1. a) A DEM and watershed delineation map of the Tyger River watershed for the pour points of samples CZ21-007 and CZ21-008 created using ArcMap software (Whipple et al, 2007). b) The Holcombe's Branch watershed DEM map and watershed delineation map created in ArcMap software (Whipple et al., 2007). The blue dots represent the centroid of each watershed, while the red dots represent the sample locations for each sub watershed.

Background

The southern Piedmont region of the Appalachian Mountains, where gradual topography and temperate to subtropical temperatures are common, was subject to harsh land use by non-indigenous immigrants (Coughlan and Nelson, 2018; Trimble, 1974). Although Native Americans farmed the Piedmont region prior to non-indigenous immigrants, it was not to the same extend. Native Americans used shallow digging tools such as backhoes, while non-indigenous immigrants used deep digging techniques such as tilling (pers. comm. Paul Schroeder, 2022). They migrated from the Coastal Plain, over the Fall Line, to the Piedmont region to expand the newfound colonies, agriculture, and economy (Costa, 1975; Coughlan and Nelson, 2018). Starting in the late 1700's and through the early 1900's, native forests were cleared for timber and crops such as tobacco, cotton, and corn (Costa, 1975; Meade and Trimble, 1974; Phillips, 1992, 2006; Trimble, 1974, 1977). The demand for tobacco in Europe resulted in the clearing and burning of forest (Costa, 1975). Plots were planted for tobacco for a number of years, abandoned for the second growth of crops, and then new land was cleared for tobacco (Costa, 1975). Cotton in the Piedmont grew to be the main crop by the 1790's, especially as time went on and slaveholding plantations became more common for cotton production (Coughlan and Nelson, 2018). Land degradation throughout the U.S., not only the CCZO, was influenced by a reorganization of plantations transitioning from owner-operated, fixed-rent, and sharecrop tenants after the Emancipation Proclamation (Coughlan and Nelson, 2018). Corn soon after became a major crop other than cotton, making it the county's main export through 1949 and covering 75% of the land in Union County (Coughlan and Nelson, 2018). As the cotton market became unstable and boll weevil infestation destroyed crops, plots of land were abandoned and

farming declined (Coughlan and Nelson, 2018). Land degradation in the 1900's became very apparent, mainly due to the cotton production in the past years and many suggest that land-owner farming techniques played a large role in the erosion of this soil (Coughlan and Nelson, 2018). Charles (1987) suggested that "an owner might not see portions of his holdings for months on end, while workers were engaged in poor cultivation practices." When you combine poor tilling and planting with heavy rainfall and rough terrain, soil erosion would be unavoidable (Trimble, 1985; Metz, 1958; Lounsbury, 1914; Zonneveld, 1989; Coughlan and Nelson, 2018). Areas of the CCZO, like Holcombe's Branch, were abandoned mostly due to economic reasons (Coughlan and Nelson, 2018). Through research on the land tenure tracts in the CCZO, it is proposed that farmers who lacked land tenure security were more likely to dismiss conservation measures, especially once the "Bankhead Cotton Act" added a 50% tax on cotton prices (Steffan et al., 2015; Coughlan and Nelson, 2018). Sharecroppers were more likely to not invest in the land, resulting in land degradation, while wealthier and actual landowners would invest some sort of conservation practice such as maintained terracing (Stone, 1996; Tarolli, 2014; Coughlan and Nelson, 2018). Farmers who lacked land security would abandon the land due to insufficient funds or a desire to invest, leading to poor landscape maintenance (Coughlan and Nelson, 2018). Plots of land in Holcombe's Branch show clear evidence of abandoned farmland by land use maps provided by Coughlan and Nelson (2018). Once the land had failed to be invested in, as well as wearied from overuse, it was abandoned with little vegetation leading to intense soil erosion (Trimble, 2008; Costa, 1975). The U.S. Soil Conservation Service determined that runoff in forest is less than 5%, while runoff in cultivated areas is 40-60% (U.S. Department of Agriculture, 1940). By the early 1900's an average of ~18 cm of soil eroded from the Calhoun Forest, South Carolina, creating massive gullies and clogging rivers and streams with sediment

(Costa, 1975; Meade and Trimble, 1974; Phillips, 1992, 2006; Trimble 1974, 1977). Soil conservation actions were put into effect in the 1940's to preserve the land for research. By using *in situ*-produced ^{10}Be cosmogenic nuclides in quartz grains, collected in Holcombe's Branch stream and Tyger River, an average basin-wide denudation rate can be calculated giving a better understanding of how human-induced landscape disturbance affects soil erosion on the millennial time scale when compared to long-term and short-term sediment yield and areally averaged hillslope erosion rates (Reusser et al., 2015; Simmons, 1993; Summerfield and Hulton, 1994; Trimble, 1977; Wilkinson and McElroy, 2007).

Geologic Setting

This study was conducted in the Calhoun Critical Zone Observatory (CCZO), an Experiential Forest within the Sumter National Forest in the southern Piedmont of South Carolina (Mallard, 2020; Wade et al., 2020). The Piedmont region of South Carolina sits at 152-305 m in elevation, in between the Blue Ridge Mountains (up to ~558 m in elevation) and the Atlantic Coastal Plain (~0-152 m in elevation) (Trimble, 2008). Within the Piedmont, there are upper and lower sections (Trimble, 2008). The upper Piedmont consists of narrow interfluves and ridges, with steeper topography (pers. comm. Paul Schroeder, 2022). The lower Piedmont consists of broad interfluves and gradual slopes (Trimble, 2008). Stretching from Virginia to Alabama, are soil series such as Cecil, Helena, Appling, Madison, Hiwassee, and Durham (Trimble, 2008). Higher in the Piedmont soil series are Haysville, Porters, and Ashe, where the topography of the Piedmont becomes steeper (Trimble, 2008). The low-gradient interfluves join to bottomland streams and rivers in the southern Piedmont are characteristic of the geography of the CCZO

(Mallard, 2020). This region consists of seasonal changes between ephemeral and perennial 1st order streams (Mallard, 2020).

The Holcombe's Branch watershed has an area of 6.06 km^2 within the CCZO (190 km^2) (Wade et al., 2020). Holcombe's Branch is part of the Broad River Basin which covers the NNW section of South Carolina. Within the Broad River Basin is the Middle Tyger River watershed (70.6 km^2). Holcombe's Branch watershed is a low-order stream that discharges into the Tyger River, and then into the Broad River within the Broad River Basin (Wade et al., 2020, fig. 1). The elevation above sea level from the headwaters to the mouth of Holcombe's Branch stream is 130.1 m (sample CCZO-6) to 109.1 m (sample CCZO-2). The Tyger River samples are at an elevation of 114.9 m upstream of HLCB (CCZO-8) and 107.2 m above sea level downstream of HLCB.

The soils within the watershed are loamy sands beneath clay-rich argillic horizons, characterized as Ultisols of mainly Appling, Madison, Cartecay, Cataula, Cecil, Hiwassee, Enon, Louisburg, and Wilkes series (Richter et al., 2000; Soil Survey Staff, 2022; fig. 4). The Ultisols developed over top of biotite gneiss/amphibolite that underwent metamorphism to granodiorite of the Wildcat Branch complex (Mallard, 2020). Alluvial legacy sediments, sediments deposited due to anthropogenic activity, were measured in mean cross-section depth at an average of 1.01 m from the surface (Wade et al., 2020). The legacy sediments, shown by LiDAR-derived 1m^2 DEM, reflect the floodplains in Holcombe's Branch (Wade et al., 2020). The thickness varies from 36 cm to 125 cm, dating back to 150 years ago using charcoal deposits (Wade et al., 2020). Below these soils is weathered saprolite, reaching an average depth of 6-15 m where gullies have been deeply down cut (Trimble, 2008). In some areas of the CCZO the bedrock age ranges from Neoproterozoic to Cambrian Cat Square terrane in some areas, while in other areas bedrock is connected to the Charlotte terrane and the Wild Cat Complex with biotite-hornblende-quartz metadiorite and

metatonalite (Fig. 2) (Huebner et al., 1977; Jordan, 2020; Dennis & Wright, 1997; Horkowitiz, 1984).

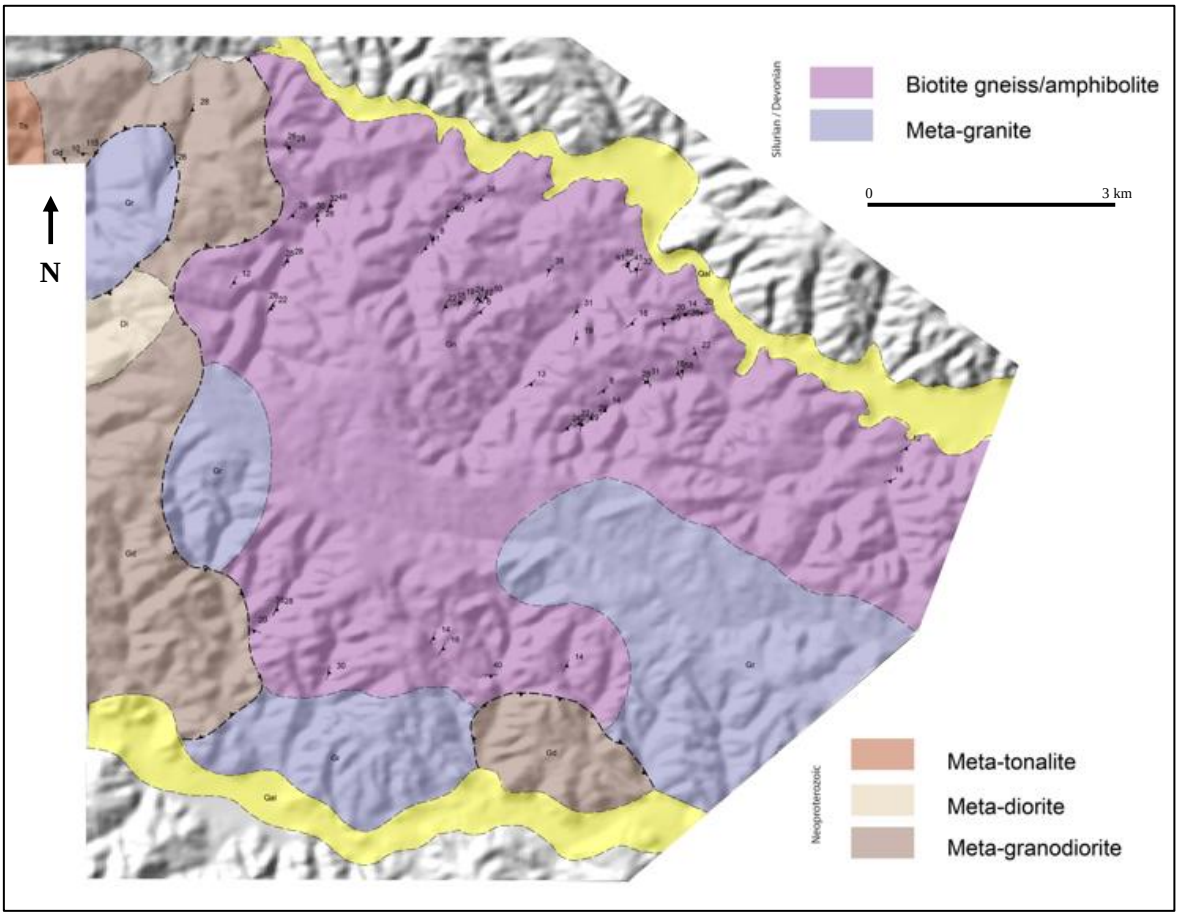

Fig. 2: Geologic map of Holcombe's Branch and the surrounding CCZO forest (Jordan, 2020).

Methods

Quartz Separation and ^{10}Be Cosmogenic Nuclide Isotope Extraction

To determine the background denudation rate in the Calhoun Forest, seven samples were collected within two watersheds by Paul Schroeder, Andy Darling, and I in February of 2021. Five of the samples were collected going upstream in Holcombe's Branch (HLCM) starting where it discharges into the Tyger River. One sample was taken from a longitudinal bar and four were taken from point bars using a small metal shovel and bag (Fig. 3). Two samples, collected in the Tyger River, were retrieved by throwing a metal pipe connected to a rope into flowing water to dredge the samples from the rivers bed load, up and downstream, where Holcombe's Branch discharges into the Tyger River (Fig. 3). Soil samples from nearby pits were also collected and used for the study of ^{26}Al and ^{10}Be. Details of sample locations, mineralogy, and other properties are described in Schroeder et al. (2022). Soil samples were combined at certain depths to give ^{26}Al and ^{10}Be concentrations for a zone within the soil profile.

Fig. 3 a) Location of sample CZ21-004, collected on the point bar (red arrow) in Holcombe's Branch. b) Location of sample CZ21-007 collected in the bedload (red arrow) of the Tyger River.

The sediment and soil samples were prepared using mineral separation techniques, where grains were sieved to 250-850 microns at the University of Vermont's Cosmogenic Laboratory (Corbett et al., 2016). Quartz grains went through two series of ultrasonic etching in hot 6N HCl to dissolve iron grain coatings and thrice in diluted (1%) HF-HNO^3 to dissolve feldspars (Corbett et al., 2016). The quartz grains were tested for purity and yield of total cations (Al and Be) using inductively couple plasma optical emission spectrometry (Corbett et al., 2016). Samples were split into two separate batches of ten, plus two blanks (Corbett et al., 2016). The purified quartz grains for the sediment and soil samples were dissolved with ~1 g of low-level ^{9}Be carrier in 100 g of concentrated HF for all samples, so that the amount of ^{9}Be can be calculated after the ^{10}Be/^{9}Be ratio is determined by the accelerated mass spectrometer (AMS) (Corbett et al., 2016). The ^{9}Be added was made at the University of Vermont with a concentration of 304 ug mL^{-1} (Corbett et al., 2016). The sediment and soil samples received an addition of 1351-1525 ug of ^{27}Al carrier (Corbett et al., 2016). Four series of $HClO^4$ additions allowed beryllium to bond to perchlorate and then heated to 230 ºC to drive off the fluoride, leaving a small orange/gold colored pellet (Corbett et al., 2016).

To prepare for the anion column chromatography, two additions of HCl were applied and evaporated to the pellet, displacing the perchlorate bond and altering it to chloride form (Corbett et al., 2016). The samples were then diluted in 5 mL of 6 N HCl to allow the column resin to separate iron ($FeCl^-$) from the other cations and transferred to a tube using a transfer pipette (Corbett et al., 2016). The sample tubes are then centrifuged to precipitate out some of the titanium, but not all (Corbett et al., 2016). The precipitated titanium was oxidized by the four perchloric acid fumings (Corbett et al., 2016).

The anion columns consist of organic resin with top and bottom frits, which protect the resin (Corbett et al., 2016). Each sample is pipetted into its given column, being sure to only pipette the liquid and leaving behind the precipitated titanium (Corbett et al., 2016). As the sample percolates through the column, the iron binds onto the resin, while the cations pass through the resin into a sample beaker (Corbett et al., 2016). A few mL of 6N HCl is passed through the columns to be sure all the cations are accounted for in the beaker (Corbett et al., 2016).

Once the $FeCl_5^-$ has been discarded, the samples can pass through the cation columns to separate out Ti, Al, Si, Mg, and Be (Corbett et al., 2016). Using a pipette to transfer the samples into the resin, the positively charged cations bond to the negatively charged resin (Corbett et al., 2016). Since titanium has the weakest bond out of the cations present, 5.78 column volumes of 0.65 M sulfuric acid are added to the cation column (Corbett et al., 2016). Due to the weak bond between the titanium cations and the resin, the bond breaks eluding titanium into a beaker (Corbett et al., 2016). The strength and amount of sulfuric acid added is not strong enough to break the bonds of the remaining cations (Corbett et al., 2016). Beryllium, having the second weakest bond, is eluded by adding 5.5 column volumes of 1.2 N HCl (Corbett et al., 2016). To reduce any boron that may be present, 7 drops of 8 M HNO_3 are added to each beaker and placed on the hot plate to evaporate overnight (Corbett et al., 2016). The magnesium cations have a slightly stronger bond to the resin than beryllium, so 10 column volumes of 1.2 N HCl are added to the resin (Corbett et al., 2016). Aluminum, having the strongest bond out of the cations here, is eluded into a beaker by adding 4 N HCl and set onto a hot plate to evaporate overnight (Corbett et al., 2016).

To re-dissolve the samples, 8 mL of 1% nitric acid is added to the beryllium and aluminum beakers, and then placed into Teflon tubes (Corbett et al., 2016). For ICP analysis of the Al and Be cations, 200 uL aliquots were taken from the sample tubes and mixed with 1% sulfuric acid (Corbett et al., 2016). The yield percentage and purity of each sample were measured through the ICP-OES (Corbett et al., 2016). Beryllium had a high mean yield of 96%. After the samples pass the ICP-OES analysis for containing a high yield of beryllium and aluminum with no impurities, one drop of methyl red was added to each tube to indicate the pH (Corbett et al., 2016). 10 drops of 30% NH_4OH are added to the sample tube, capped, and shaken (Corbett et al., 2016). If there is no color change, then one more drop is added and shaken again. This was repeated until the beryllium and aluminum samples turn from red to yellow/green and stays that color, reaching a pH of 7 (Corbett et al., 2016). One more drop was added of 30% NH_4OH to reach a pH of 8 (Corbett et al., 2016). This process of adding the 30% NH_4OH is neutralizing the 1% nitric acid and the 0.65 M sulfuric acid in the sample tube (Corbett et al., 2016). The sample is then centrifuged to precipitate BeOH and AlOH gels (Corbett et al., 2016). Each sample was then altered to BeO and AlO by burning off the hydroxides (Corbett et al., 2016).

Upon completion of extracting the beryllium and aluminum from the quartz grains, the extracted isotopes were analyzed at Purdue University's PRIME lab to measure the $^{27}Al/^{26}Al$ $^{10}Be/^{9}Be$ isotopic ratio using an Accelerated Mass Spectrometer (AMS). The ratios were normalized to standard 07KNSTD3110, with an assumed ratio of 2850×10^{-15} (Nishiizumi et al., 2007). Using processed blanks for each batch of samples, the normalized ratios were corrected (Corbett et al., 2016).

Watershed Delineation

To model the denudation rate for each sample, 1/3 arc sec 10 m DEM files were downloaded in ArcMap to create accumulation flow maps and flow direction maps (U.S. Geological Survey, 2022; Whipple et al., 2007). The coordinates for each sample were added and run as pourpoints (Whipple et al., 2007). The watershed tool was run using the pourpoints and the flow direction inputs, which created sub-watersheds as polygon shape files (Whipple et al., 2007). The file shows the area of the watershed for each sample pourpoint to the headwater (Fig. 1). The area and centroids were calculated from the polygon shapefiles for each sample/pourpoint (Whipple et al., 2007). The centroid, coordinates, atoms/gram of ^{10}Be, quartz density, and standardized values from the accelerated mass spectrometer, were combined to calculate the denudation rate for each sample in an online calculator, CRONUS, created at the University of Washington (Whipple et al., 2007; http://hess.washington.edu, table 1)

Watershed Erosion Prediction Project (WEPP): sediment yield

Annual sediment yields were calculated in the online version of WEPP (Flanagan and Nearing, 1995) to determine the amount of sediment transported within Holcombe's Branch. The outlet of Holcombe's Branch was pinpointed to create a delineated watershed in the program. Inputs such as; climate station (UNION 7 SW station), soil type (all soil types, figure 4), land use (thin or young forest), simulation type (watershed and flow paths), year to simulate (1 year), soil loss tolerance (T-value = 5) were used to calculate the annual sediment yield within the watershed. To compare the sediment yield to the long-term ^{10}Be derived denudation rate, conversions were completed to reflect the sediment yield in meters per million years using a bulk soil density of Holcombe's Branch of 1.5 g/cm^3 (pers. comm. Paul Schroder, 2023).

K-Factor

Another look at the soils erodibility in Holcombe's Branch was to determine how susceptible the soil is to erosion, the K-factor (Foster et al., 1981). In ArcMap, the soil erodibility (K-factor) can be modeled (Fig. 5). The K-Factor was determined using data collected on the Web Soil Survey website, where it was calculated based on the sand, clay, and silt percentages for Holcombe's Branch watershed (Soil Survey Staff, 2022). By adding the K-values to the attribute table, an average soil erodibility value was calculated and modeled (Fig. 5).

Results

Holcombe's Branch and Tyger River

Background erosion rates, measured by *in situ*-produced ^{10}Be cosmogenic nuclide isotopes, show that the sediments in Holcombe's Branch and the Tyger River are homogenized. As organisms and hillslope processes rework the sediment, the concentration of transported sediments stay constant (Jungers et al., 2009; Reusser et al., 2015). The average ^{10}Be concentration for Holcombe's branch sediments is measured at 3.70 ± 0.07 (atoms/g of quartz x 10^5) and the average concentration in the Tyger River sediments is measured at 3.61 ± 0.01 (atoms/g of quartz x 10^5) (Table 2). Both averaged concentrations are close in value with only a 0.09 (atoms/g of quartz x 10^5) difference between the two tributaries. The concentration of Holcombe's Branch and Tyger River samples resulted in a basin-wide average of ^{10}Be concentration at 3.67 ± 0.08 (atoms/g x 10^5). Individual concentrations for each sample are shown in table 2 and are plotted in figure 7.

Statistical analysis for Holcombe's Branch and the Tyger River watersheds were conducted on each sub-watershed using a 10 m 1/3 arc sec mosaiced DEM, extracted in ArcMap

GIS software (U.S. Geological Survey, 2022; Whipple et al., 2007). Sub-watershed CZ21-002, having the largest catchment due to the location being furthest downstream, has the largest area between the sub watersheds. The mean elevation for each sub-watershed was extracted in ArcMap for CRONUS calculation. Holcombe's branch sub-watersheds have a mean elevation ranging from 154 m at CZ21-002 to 169 m at CZ21-006. The Tyger River sub-watersheds have a mean elevation of 243 m for CZ21-007 and 244 m for CZ21-008. As CZ21-007 is further downstream, it has a larger sub-watershed compared to CZ21-008. The centroidal latitude and longitude were extracted from each sub-watershed in Holcombe's Branch and the Tyger River.

CRONUS, an online calculator (Balco et al., 2008), determines the average erosion rate using cosmogenic nuclide concentrations, centroid coordinates, mean elevation, depth of the sample, shielding correction, the density of the mineral, and AMS standardization values (Table 1). The elevations and centroids were extracted from ArcMap. The sediment samples were collected on the surface of the stream bed, making the input values for CRONOUS at 0.1 cm. Quartz grains were separated from the bulk samples, with a density of 2.65 g/cm^3. The shielding correction was set at 1. Sample ratios were normalized to standard 07KNSTD (Nishiizumi, 2004). The basin-wide average denudation rate in the Broad River Basin is measured at 7.1 ± 0.2 m/Ma, as calculated through the CRONUS calculator (http://hess.washington.edu).

Holcombe's Branch sediment yield

The long-term sediment yield for Holcombe's Branch, from the WEPP online application, was measured at 161.5 m/Ma.

K-Factor

The K-factor was extracted in ArcMap by averaging the sand, silt, and clay fractions, which reflect the susceptibility of soil particles to detach and transport by rainfall and runoff. The sand percentage for the watershed was collected from the Web Soil Survey, at 66 % (Soil Survey Staff, 2022). The clay fraction was 12 % of the soil series and silt was measured at 19 % (Soil Survey Staff, 2022). The Web Soil Survey soil data included the K-factor values in Holcombe's branch, and when averaged together, resulted in a value of 0.22 in the watershed, ranging from 0.10 to 0.28 (Soil Survey Staff, 2022; figure 4 and 7). Appling loamy sand has a rating of 0.10, Cartecay-Toccoa complex has a rating of 0.15 (Soil Survey Staff, 2022). Cataula and Cecil have a rating of 0.24 (Soil Survey Staff, 2022). Enon and Wilks sandy loam and soil has a rating of 0.28 (Soil Survey Staff, 2022). Hiwassee, Louisburg, and Madison sandy loam has a rating of 0.17 (Soil Survey Staff, 2022). Hiwassee sandy clay loam has a rating of 0.20 (Soil Survey Staff, 2022). Connections to the soil erodibility factor with the interfluve and farming locations are discussed below.

Soil Pits

Soil samples at depth were collected in a previous study (Schroeder et al., 2022) and ^{26}Al and ^{10}Be cosmogenic nuclide isotopes were measured for each sample. ^{26}Al and ^{10}Be concentrations have a non-linear relationship to depth (Granger et al., 2013). R1C2, R1C3, and R8H1 soil pit samples have the greatest ^{26}Al and ^{10}Be concentrations closer to the surface compared to concentrations deeper in the profile (Fig. 8 and 9). Sample R1C2 had an ^{26}Al concentration of 1.96×10^6 atoms/g^{-1} and a ^{10}Be concentration of 4.157×10^5 atoms/g^{-1} in the upper 80 cm zone of the profile. At depth intervals of 113–400 cm, the ^{26}Al concentration is 4.51

x 10^5 atoms/g^{-1} and the ^{10}Be concentration is 8.12 x 10^4 atoms/g^{-1}. At depth intervals of 500–800 cm, the ^{26}Al concentration is 1.91 x 10^5 atoms/g^{-1} and the ^{10}Be concentration is 4.09 x 10^4 atoms/g^{-1}. The concentrations continue to show a decrease in concentrations as samples move down the profile (Fig. 8 and 9). Deep soil samples from sites R1C2, R1C3, R7H1, R7H2, R7P2, and R8H1 had a combined depth zones ranging from 500-900 cm in certain profiles (Schroeder et al., 2022). Sample pits R1C2, R1C3, R7H1, R7P2, and R8H1 had an average ^{26}Al concentration of 1.98 x 10^5 and ^{10}Be concentration of 3.15 x 10^4 (Fig. 10 and 11). Sample R7H2 is an outlier with a much higher concentration in ^{26}Al (3.05 x 10^6 atoms/g^{-1}) and ^{10}Be (4.50 x 10^5 atoms/g^{-1}) (Fig. 10 and 11; Table 3).

The cosmogenic ratio of ^{26}Al/^{10}Be in the soil samples shows an increased ratio closer to the surface and a decreased ratio deeper in the profile due to decay through time (pers. comm. Andy Darling, 2023). R1C2 had a surface ratio of 4.71 ± 0.21, R1C3 had 5.24 ± 0.22, and R8H1 had 7.10 ± 0.49 (Fig. 13). The ratios for the deeper profile depths were measured, but to be comparable to canonical decay rates they need to be surface samples within the top 1 meter of soil or sediment (Corbett et al., 2017). Only three soil pits had ratios in the top 1 meter (Fig. 13). The canonical standard value for ^{26}Al/^{10}Be ratio is ~6.75, which had experienced an increase from ~6.1 (Lal, 1991) due to new AMS standards (Nishiizumi et al, 2007) and a revision to the ^{10}Be ½ -life (Chmeleff et al., 2010).

Discussion

K-factor

The soils in Holcombe's Branch range from 0.10 to 0.28 on the K-factor scale (Soil Survey Staff, 2022; figure 5). This erodibility factor describes how susceptible the soil is to

detach from runoff (Soil Survey Staff, 2022). When you compare the K-factor to the soil map, you can see that the most erodible soils are Wilks sandy loam and soil, at 0.28 (Soil Survey Staff, 2022). This corresponds to the high K-factor values shown in red on the K-factor map (fig. 5). A reason the south eastern side of Holcombe's Branch has more erodible soils is due to how the area was previously farmed (Coughlan et al., 2017). By using LiDAR imaging, evidence of pre-1940 agricultural farming in the watershed is shown by contour terraces. The contour terraces are only seen on the southeastern side of the stream, where the soils have a higher K-factor (Soil Survey Staff, 2022; U.S. Geological Survey, 2022).

Sediment Yield and Erosion Rates

The long-term sediment yield for Holcombe's Branch, calculated by WEPP, indicates that the area is transporting sediment at a greater rate than the background sediment yield data determined by Simmons (1993) in forested areas of the Blue Ridge (n=3), Piedmont (n=2), Coastal Plain (n=2) regions of North Carolina (Table 5). The background sediment yields represent undisturbed/uncultivated areas, whereas Holcombe's Branch (Piedmont) had been severely cultivated by non-indigenous people for the past > 200 years (Coughlan and Nelson, 2018). Blue Ridge forest sediment yields range from 7.2 – 65.4 m/Ma (Simmons, 1993), significantly lower than what is calculated for Holcombe's Branch (161.5 m/Ma). This represents how poor farming practices can drastically increase the rate at which soil is transported. Forested areas with minor development (mean = 51 m/Ma) showed a lower sediment yield than Holcombe's Branch between the Blue Ridge (n=4), Piedmont (n=2), and Coastal Plain (n=1).

Statistics were conducted on the long-term sediment yield data, converted from the annual sediment yield data found by Simmons (1993). By conducting t-tests, all forested land

had a mean long-term sediment yield of 7.7 m/Ma with a lower 95% confidence interval of 3.3 m/Ma and upper interval of 12.1 m/Ma (p-value = 0.005) (Simmons, 1993), providing a lower, long-term, sediment yield than the long-term sediment yield for Holcombe's Branch, 161.5 m/Ma. The forested regions with minor development within the Piedmont and Coastal Plain have a long-term mean of 30.9 m/Ma with a lower 95% confidence interval of 12.8 m/Ma and upper interval of 48.9 m/Ma (p-value = 0.005) Rural agriculture regions within the Piedmont and Coastal Plain have a long-term sediment yield mean of 27.9 m/Ma, with a lower limit of 19.4 m/Ma and an upper limit of 36.2 m/Ma (p-value = 9.9×10^{-8}). Comparing the mean sediment yields from the tributaries in different land covers located in the Blue Ridge, Piedmont, and Coastal Plain of North Carolina (Simmons 1993), shows that Holcombe's Branch is eroding at a faster rate than the mean of the three physiographic provinces (Appendix A).

Considering the drainage area of Holcombe's Branch (6.06 km^2), it is more comparable to data retrieved from Beetree Creek (14.1 km^2) within the forested area of the North Carolina Blue Ridge province (Simmons, 1993, table 5). Beetree Creek has a long-term sediment yield rate of 7.2 m/Ma, reflecting an order of magnitude lower rate of sediment transportation for an area that is undisturbed and uncultivated. It is important to point out that there is a decrease in sediment yield when there is an increase in drainage area (pers. comm. David Leigh, 2023). The difference in drainage area between Beetree Creek and Holcombe's Branch stream is not large enough to account for the order of magnitude difference in sediment yields. The severely cultivated Holcombe's Branch watershed is the cause of such high inputs of sediment throughout the tributary, compared to undisturbed and forested regions of the Carolinas (Simmons, 1993, table 5). Dutchman's Creek, located in a forested area of the North Carolina Piedmont region, has a drainage area of 8.9 km^2 and a long-term sediment yield of 9.5 m/Ma (Simmons, 1993),

significantly lower than the cultivated Holcombe's Branch watershed. Flat Creek, located in a forested area of the North Carolina Coast Plain has a drainage area of 19.8 km^2, with a long-term sediment yield of 14.0 m/Ma (Simmons, 1993), much less than the sediment yield of Holcombe's Branch (Table 5).

Long-term sediment yields closer to the yield of Holcombe's Branch were located in rural agricultural lands within the Piedmont and Coastal Plain (Simmons, 1994). The Dan River near Wentworth has a sediment yield of 102.7 m/Ma (Simmons, 1994), which is on the same order of magnitude as Holcombe's Branch (Table 5).

Long-term sediment yield data, explained in Wilkinson and McElroy (2007), has put into perspective how much sediment is transported to the ocean by each continent and on a global scale. Globally, the current mean farmland denudation rate is ~600 m/Ma, which is reflective of mostly low elevated areas (<350 m above sea level) (Wilkinson and McElroy, 2007). Areally averaged erosion rates on hillslopes during peak agricultural use in 1900 (~950 m/Ma) is on the same order of magnitude as the global farmland denudation of ~600 m/Ma (Wilkinson and McElroy, 2007). The global average sediment yield was measured at a rate of ~60 m/Ma (Ludwig et al., 1996; Summerfield and Hulton, 1994; Wilkinson and McElroy, 2007), aligning well with the sediment yield for the southern Appalachian Piedmont (~53 m/Ma), calculated from pre-1950 data (Trimble, 1977).

Along the passive margins of the United States, the lowest rate of erosion was measured at 7.21 m/Ma for elevations below 350 m of sea level, with increasing erosion rates (~0.15%) for every one meter in increased elevation (Summerfield and Hulton, 1994; Wilkinson and McElroy, 2007). *In situ*-produced ^{10}Be cosmogenic nuclide isotopes, extracted from quartz grains in the stream and river sediments of Holcombe's Branch and the Tyger River, show a background

average denudation rate of 7.1 ± 0.2 m/Ma, aligning well with the long-term erosion rate discussed by Wilkinson and McElroy (2007). When compared to Reusser et al (2015), mid-basin *in situ*-produced ^{10}Be background erosion rates reflects consistency in at least two of the basins in southern Appalachian Piedmont (Table 4). The Oconee Basin in Georgia has a similar erosion rate of 7.31± 0.6 m/Ma, as well as similar ^{10}Be concentrations to Holcombe's Branch (CZ21-006), 4.6 ± 0.07 (atoms/g of quartz x 10^5) for sample CZ21-006 and 4.83 ± 0.1 (atoms/g of quartz x 10^5) for the Oconee (Reusser et al., 2015, table 4). The Roanoke basin in Virginia has a faster erosion rate than the Broad and Oconee with an average of 6.36 ± 5 m/Ma, but on the scale of a million years, they are similar in comparison (Reusser et al., 2015, table 4).

Within Holcombe's Branch and the Tyger River, ^{10}Be concentrations and their individual denudation rates for each sub-watershed are consistent with each other (Table 2). The reason sample CZ21-006 has a higher concentration, and therefore a slower erosion rate (5.4 m/ma), is because higher on the interfluves, where the hillslope angle is lower, the rate of erosion is decreased (pers. comm. Paul Schroeder and Andy Darling, 2023). As time continues, sediment on higher elevated sections of the interfluve erodes slower, resulting in an increase of cosmogenic nuclides produced in *in situ*-quartz grains (Granger et al., 2013). From the concentration and erosion rate for sample CZ21-006, it is interpreted to have been deposited in the stream at a later time in history than the samples collected downstream. As the hillslope gradient increases from the headwater to the outlet, denudation rates increase slightly, but not enough to differentiate between them (Granger, 1996; pers. comm. Paul Bierman, 2022). These rates are still showing homogenized concentrations and denudation rates between the sub-watersheds (pers. comm. Paul Bierman, 2022). Sample CZ21-007 and CZ21-008, collected from the Tyger River bedload, are consistent with Holcombe's Branch ^{10}Be cosmogenic nuclide

concentrations and erosion rates. In 2017, Reusser et al. did a study to determine how dammed and undammed streams affect the concentrations in quartz grains. By comparing the ^{10}Be erosion rates with the average slope of the catchment in undammed streams versus dammed streams, they found that if a sample is collected further than 25 km downstream of a dam then the rates reflect the basin-wide erosion rate rather than smaller individual locations or watersheds around the dam (Reusser et al., 2017). Due to the severity of the erosion created by non-indigenous people, the sediment in the Tyger River is a mix of upstream sediment and sediment transported from the interfluves in the CCZO and surrounding Union County. There are no dams within 25 km of the Tyger River samples, as well as no dams at all in Holcombe's Branch. The concentration and erosion rate in Holcombe's Branch are consistent with the Tyger River samples, reflecting that the dams upstream of the Tyger River (>25 km) do not affect the dosage of *in situ*-produced ^{10}Be cosmogenic nuclides (Reusser et al., 2017). With that being said, the Holcombe's Branch and Tyger River erosion rates are precise, reflecting the two watersheds had been eroding at the same rate 10,000 plus years ago.

Accelerated historic deposition in Holcombe's Branch is due to post-settlement farming (Trimble, 1977) and in a past study, ^{137}Cs and ^{210}Pb isotopes were measured in the CCZO to determine legacy sediment accretion rates (Wade et al., 2020). A 60-year accretion rate, measured by ^{137}Cs isotopes, reflects a decrease in hillslope eroded legacy sediments towards the headwater of Holcombe's Branch (Wade et al., 2020). At a distance of 1.4-2.0 km upstream from the outlet where Holcombe's Branch discharges into the Tyger River, the accretion rate was 0.019 cm/year (190 m/Ma) (Wade et al., 2020). The deposition of these sediments increased downstream, at the rate of 0.21 cm/year (2,100 m/Ma) (0.4 km upstream of the outlet) (Wade et al., 2020). By using ^{210}Pb isotopes, legacy sediments dating back to 100-150 years ago revealed

that deposition was decreasing at the headwaters as well, with a higher accumulation of sediment transported further downslope due to human activity (2.0 km upstream = 0.128 cm/year; 1.3 km upstream = 0.201 cm/year; 0.4 km upstream = 0.642 cm/year (1289; 2010; 6420 m/Ma, respectively) (Wade et al., 2020). At the headwater of the watershed, ^{137}Cs peaks indicated less deposition when compared to the downstream deposits for the sixty-year accretion rate, while ^{210}Pb peaks showed an even smaller accretion rate at the headwater to the outlet (Wade et al., 2020). This suggests that in the 20th century, Holcombe's Branch experienced a decrease in legacy sediments deposited moving downslope, as post-1964 ^{137}Cs measurements were low (Wade et al., 2020). Tree trunk age and locations within the watershed, showed that the rate of sediment accretion was accelerated during peak farming when compared to the rates derived from ^{137}Cs and ^{210}Pb isotopes (Wade et al., 2020).

Soil Pits

Soil samples in the CCZO were collected at depths down to 900 cm to measure ^{26}Al and ^{10}Be cosmogenic nuclide concentrations (Schroeder et al., 2022). Due to sample mass restraints, certain depth samples were amalgamated to represent a depth zone of concentrations. As expected, the samples closer to the surface in pits R1C2, R1C3, and R8H1 have a greater amount of ^{26}Al and ^{10}Be concentration (Fig. 8 and 9). R1C3, when compared to R1C2, is further down slope on the interfluve where erosion is greater and the mobilization of soil through creep and sheet wash is greater (pers. comm. Paul Schroeder, 2023). R1C2 has a smaller dosage of cosmogenic nuclides than R1C3 (Fig 8 and 9). It is expected that higher on the interfluve, the dosage would be greater, where the soil has been less mobilized allowing for a greater amount of cosmic ray accumulation over time (Granger, 1996). The thickness of the soil profile to the

saprolite at R1C3 is thinner than the thickness at R1C2 (Fig. 12). As bioturbation and pedological processes occur, the mobilization of soil is less at R1C2 and greater downslope at R1C3. If this was true than R1C2 would have a higher concentration of ^{26}Al and ^{10}Be, compared to the downslope profile, R1C3. From the results, this is not the case. Two assumptions can be made from the results and location of the soil pits. R1C2 may have been cultivated at a greater degree than downslope at R1C3. According to the land tenure map, the two soil pits were located in a fixed rent tenant farm field (Coughlan and Nelson, 2017). Fixed rent tenants, compared to landowners, did not practice conservation as well (Coughlan and Nelson, 2017). It is assumed that the farming techniques used in R1C2 could have overturned quartz grains with less cosmic dosage from deeper tilling and more erosive farming practices, resulting in a smaller ^{26}Al and ^{10}Be concentration in R1C2 if R1C3 was not tilled as deeply and eroded as quickly.

Production of ^{10}Be in the upper meter is fairly constant across all three sites. Although each site has a different depth range of amalgamated soil, R1C2 has a ^{10}Be concentration of 4.2 x 10^5 across a depth zone of 0-80 cm (atoms/g of quartz x 10^5) (Fig. 9). Soil pit R1C3 has a ^{10}Be concentration of 6.7 x 10^5 (atoms/g of quartz x 10^5) for a depth range of 0–18 cm and a concentration of 4.2 x 10^5 (atoms/g of quartz x 10^5) for depths 58–86 cm, suggesting that the top of the first meter of soil, at some degree, is getting a larger dosage of ^{10}Be (Fig. 9). The average of R1C3 ^{10}Be concentration for 0 – 86 cm is 5.5 x 10^5 (atoms/g of quartz x 10^5) (Fig. 9).

The deep soil profile samples from all six sites show a very consistent production of ^{10}Be except for one outlier (R7H2) (Fig. 10 and 11). The concentration of cosmogenic nuclides in the deep sections of the profile is a mix of spallation and muon production (Granger et al., 2013). The ^{26}Al and ^{10}Be concentration at depths past 500 cm is interpreted to be a product of mostly muon production, because cosmogenic nuclides through the spallation effect are not able to

penetrate the earth's surface at these deep depths (Granger et al., 2013). The outlier sample, R7H2, has a ^{26}Al concentration of 3.1 x 10^5 (atoms/g of quartz x 10^5) and a ^{10}Be concentration of 4.5 x 10^5 (atoms/g of quartz x 10^5), which is much higher in concentration than the rest of the deep profile samples. The location of R7H2 is southwest of Holcombe's Branch, on the southwest side on the Enoree River, the southward adjacent river to the Tyger River. One assumption as to why the cosmogenic dosage is higher at R7H2 deep depths is due to the mineralogy of the saprolite compared to the pits near the Tyger River (Schroeder et al., 2022). Schroder et al (2022) explains that this pit shows extensive weathering of the saprolite, suggesting the parent rock differs from the sites closer to the Tyger river, and is potentially older in age (R1C2, R1C3, R2H1, and R8H1). Geologic mapping of the CCZO shows a variation between intermediate and felsic rock, so in regard to the higher concentration of cosmogenic concentration in R7H2, this could have been due to the soil forming at an earlier time and land use practices between all the pit locations (Jordan, 2020; Schroeder et al., 2022).

The $^{26}Al/^{10}Be$ ratios in the CCZO soil pits, R1C2 and R1C3, are lower than the ratio in R8H1 (Table 3, figure 13). The average of all three ratios is 5.6, showing a higher decay rate compared to the canonical value of ~6.75, which was measured in areas such as Greenland and the Rocky Mountains (Nishiizumi, 2017; Chmeleff et al, 2010; Corbett et al., 2017). Corbett et al. (2017) measured the ratio of granitic outcrops in Greenland, resulting in a ratio of 6.79-6.82 (Corbett et al., 2017). Although the CCZO values are lower, it is likely due to the latitude and altitude of the CCZO and the age of soil formation compared to Greenland, meaning the values shouldn't be equal (Corbett et al., 2017). Spatially, the ratios vary across Earth, and since cosmogenic ratios have yet to be measured in various regions, there are not many values to compare the decay rates to for the CCZO (Corbett et al., 2017). The CRONUS online calculator

uses the canonical value of 6.75 to determine erosion rates and production rates (Corbett et al., 2017).

Conclusion

The Broad River Basin, by measurement of ^{10}Be cosmogenic nuclide isotopes, is eroding at an average rate of 7.1 ± 0.2 m/Ma. This background denudation rate records the natural rate, but with Native American influence. It is hard to say how much the Native Americans truly influenced the landscape, but we do know that it was not as detrimental to the rate of denudation compared to non-indigenous immigrants. Trimble (1977) suggested that the soil erosion dating back to at least 10 ka was spatially uniform, as the Broad River Basin ^{10}Be derived denudation rates reflect. Although there were times of increased and decreased erosion due to climate conditions and possible Native American influence, it was not as severe as when non-indigenous immigrants began deforesting and farming the southern Appalachian Piedmont (Trimble, 1977). This is indicated by ^{10}Be cosmogenic nuclide measured denudation rates studied in this paper, which is compared to published and measured sediment yields and hillslope erosion rates (Simmons, 1993; Summerfield and Hulton, 1994; Wilkinson and McElroy, 2007; Trimble, 1977). The bulk of eroded sediments transported down slope was brought into rivers and streams, but mainly stored in valley bottoms and toe slopes in the Calhoun and around the Piedmont regions (Meade, 1982; Trimble, 1974). Even though denudation rates were far less prior to the 1700's, rivers and streams were not transporting all this eroded material (Trimble, 1974). It is unknown how long it may take to transport these sediments into a tributary system and eventually into the oceans, but it is likely to take many decades if not centuries (Jackson et al., 2005). It may take millennia for this to happen, but the exact time period is still undetermined (Jackson et al,. 2005). Unfortunately, due to the legacy sediment stored in valley bottoms and toe

slopes, the sediment being transported downstream will remain elevated (Meade, 1982; Phillips, 2006). From ^{137}Cs and ^{210}Pb measurements, there is evidence that the deposition of legacy sediments has decreased, even though it remains elevated to background conditions (Meade, 19882; Phillips, 2006; Wade et al., 2020). Over time, and with conservation measures intact, the rate of legacy sediment deposition will continue to decrease (Wade et al., 2020).

Since the US government started conservation action in the 1940's, sediment yields in the tributaries have decreased (Reusser et al., 2015). The CCZO has begun to grow a secondary forest due to soil conservation action (pers. comm. Paul Schroeder, 2022). Between 1910 and 1934, sediment yield within Ocmulgee River measured a ~74 m/Ma basin wide average erosion rate (Meade and Trimble, 1974). After conservation, between 1967 and 1972, sediment yield values dropped to ~ 10 m/Ma, aligning closer to ^{10}Be cosmogenic nuclide measured denudation rates (~11 m/Ma) (Reusser et al., 2015; Trimble, 1977). Their research suggest that soil conservation does in fact reduce sediment yield and erosion back to background rates, prior to non-indigenous immigrant related erosion (Meade and Trimble, 1974; Reusser et al., 2015).

Through sediment yield values and *in situ*-produced ^{10}Be cosmogenic nuclide measured erosion rates, land use practice by humans explicitly impact the rate of erosion (Hicks et al., 2000; Marsh, 1882; Syvitski et al., 2005). Although humans do and have impacted the rate of erosion, conservation measures can reverse these effects to reflect an equilibrium rate of erosion (Reusser et al, 2015). Due to the long ½ -life of ^{26}Al and ^{10}Be cosmogenic nuclides and the non-linear relationship of cosmogenic concentration to depth, this is an excellent method to understand and manage landscape and landscape evolution (Reusser et al., 2015).

CHAPTER 3

CONCLUSION AND FUTURE RESEARCH

The main conclusion that can be drawn from this research is that the background (natural) erosion rate eroded at a rate of 7.1 ± 0.2 m/Ma, by measurement of *in situ*-produced ^{10}Be cosmogenic nuclides showing an increase in erosion through legacy influence. When compared to post settlement areally average rates of erosion (~950 m/Ma), sediment yield data (measured: 161.5 m/Ma and published), and ^{137}Cs and ^{210}Pb isotope data, the rate increased through the 18th, 19th, and mid 20th centuries due to non-indigenous immigrant influence (Reusser et al., 2015; Wade et al., 2020). Due the Soil Conservation Service taking initiative to start conservation measures in the 1940's, as seen through ^{137}Cs and ^{210}Pb accretion rates, soil denudation rates can be reversed to reflect the background rate of erosion (U.S. Department of Agriculture, 1940; Wade et al., 2020). As the CCZO sprung a secondary regrowth of forests, soil mobilization stabilized. Landscape management tactics can be aided by knowledge of the background denudation rates to improve conservation measures in other areas subjected to harsh anthropogenic influences.

Future research on denudation rates and decay rates, derived from ^{26}Al and ^{10}Be cosmogenic nuclide concentrations at depth, can further aid the understanding of soil and cosmogenic nuclide production rates in critical zone science, the Broad River Basin, and the southern Appalachian Piedmont. Future work should focus on delineating sub watersheds for the soil pit locations, so that denudation rates can be calculated in CRONUS. Soil pits, especially R1C2 and R1C3, can further be looked at as to why the higher elevated pit (R1C2) on the

interfluve produced less concentrations of cosmogenic nuclides compared to downslope pits (R1C3).

References

Balco, G., Stone, J. O., Lifton, N. A., & Dunai, T. J. (2008). A complete and easily accessible means of calculating surface exposure ages or erosion rates from ^{10}Be and ^{26}Al measurements. Quaternary geochronology, 3(3), 174-195.

Bierman, P., & Steig, E. J. (1996). Estimating rates of denudation using cosmogenic isotope abundances in sediment. Earth surface processes and landforms, 21(2), 125-139.

Brown, E. T., Stallard, R. F., Larsen, M. C., Raisbeck, G. M., & Yiou, F. (1995). Denudation rates determined from the accumulation of in situ-produced 10Be in the Luquillo Experimental Forest, Puerto Rico. Earth and Planetary Science Letters, 129(1-4), 193-202.

Burrough, P. A., McDonnell, R. A., & Lloyd, C. D. (1998). *Principles of geographical information systems*. Oxford university press.

Charles, A. D. (1987). The Narrative History of Union County. *South Carolina*, *427*.

Chmeleff, J., von Blanckenburg, F., Kossert, K., & Jakob, D. (2010). Determination of the ^{10}Be half-life by multicollector ICP-MS and liquid scintillation counting. *Nuclear Instruments and Methods in Physics Research Section B: Beam Interactions with Materials and Atoms*, *268*(2), 192-199.

Corbett, L. B., Bierman, P. R., Rood, D. H., Caffee, M. W., Lifton, N. A., & Woodruff, T. E. (2017). Cosmogenic ^{26}Al/^{10}Be surface production ratio in Greenland. *Geophysical Research Letters*, *44*(3), 1350-1359.

Corbett, L. B., Bierman, P. R., & Rood, D. H. (2016). An approach for optimizing in situ cosmogenic 10Be sample preparation. *Quaternary Geochronology*, *33*, 24-34.

Costa, J. E. (1975). Effects of agriculture on erosion and sedimentation in the Piedmont Province, Maryland. Geological Society of America Bulletin, 86(9), 1281-1286.

Coughlan, M. R., Nelson, D. R., Lonneman, M., & Block, A. E. (2017). Historical land use dynamics in the highly degraded landscape of the Calhoun Critical Zone Observatory. *Land*, *6*(2), 32.

Coughlan, M. R., & Nelson, D. R. (2018). Influences of Native American land use on the colonial Euro-American settlement of the South Carolina Piedmont. *PLoS One*, *13*(3), e0195036.

Dennis, A. J., & Wright, J. E. (1997). The Carolina terrane in northwestern South Carolina, USA: Late Precambrian-Cambrian deformation and metamorphism in a peri-Gondwanan oceanic arc. Tectonics, 16(3), 460-473.

Eberly, D. (1999). Least Squares Fitting of Data, paper via Geometric Tools.

Flanagan, D. C., & Nearing, M. A. (1995). USDA-Water Erosion Prediction Project: Hillslope profile and watershed model documentation. *Nserl* Rep, 10, 1-123.

Foster, G. R., McCool, D. K., Renard, K. G., & Moldenhauer, W. C. (1981). Conversion of the universal soil loss equation to SI metric units. *Journal of Soil and water conservation*, *36*(6), 355-359.

Granger, D. E., Kirchner, J. W., & Finkel, R. (1996). Spatially averaged long-term erosion rates measured from in situ-produced cosmogenic nuclides in alluvial sediment. *The Journal of Geology*, *104*(3), 249-257.

Granger, D. E., Lifton, N. A., & Willenbring, J. K. (2013). A cosmic trip: 25 years of cosmogenic nuclides in geology. *Bulletin*, *125*(9-10), 1379-1402.

Haggett, P. (1961). Land use and sediment yield in an old plantation tract of the Serra do Mar, Brazil. *The Geographical Journal*, *127*(1), 50-59.

Heimsath, A. M., Furbish, D. J., & Dietrich, W. E. (2005). The illusion of diffusion: Field evidence for depth-dependent sediment transport. *Geology*, *33*(12), 949-952.

Hicks, D. M., Gomez, B., & Trustrum, N. A. (2000). Erosion thresholds and suspended sediment yields, Waipaoa River basin, New Zealand. *Water Resources Research*, *36*(4), 1129-1142.

Hofmann, H. J., Beer, J., Bonani, G., Von Gunten, H. R., Raman, S., Suter, M., ... & Zimmermann, D. (1987). 10Be: Half-life and AMS-standards. Nuclear Instruments and Methods in Physics Research Section B: Beam Interactions with Materials and Atoms, 29(1-2), 32-36.

Hofmann-Wellenhof, B., Lichtenegger, H., & Collins, J. (2012). *Global positioning system: theory and practice*. Springer Science & Business Media.

Hooke, R. (1994). On the efficacy of humans as geomorphic agent. *GSA Today*, *4*(9), 223-225.

Horkowitz, J. P. (1984). Geology of the Philson Crossroads 7.5 minute quadrangle. South Carolina—The nature of the boundary separating the Inner Piedmont from the Carolina/Avalon terrane in central-north western South Carolina [MS thesis]: Columbia, South Carolina, University of South Cardina.

Huebner, M. T., Hatcher, R. D., & Merschat, A. J. (2017). Confirmation of the southwest continuation of the Cat Square terrane, southern Appalachian Inner Piedmont, with implications for middle Paleozoic collisional orogenesis. *American Journal of Science*, *317*(2), 95-176.

Jackson, C. R., Martin, J. K., Leigh, D. S., & West, L. T. (2005). A southeastern piedmont watershed sediment budget: Evidence for a multi-millennial agricultural legacy. *Journal of Soil and Water Conservation*, *60*(6), 298-310.

Jordan, B. (2020). *Geology of the Calhoun Critical Zone Observatory* (Doctoral dissertation, University of Georgia).

Jungers, M. C., Bierman, P. R., Matmon, A., Nichols, K., Larsen, J., & Finkel, R. (2009). Tracing hillslope sediment production and transport with in situ and meteoric 10Be. Journal of Geophysical Research: Earth Surface, 114(F4).

Lounsbury, C.; McLendon, W.E.; Kerr, J.A. (1914), *Soul Survey of Union County, South Carolina*; US Department of Agriculture, Bureau of Soils: Washington, DC, USA.

Mallard, J. (2020). *Hydrologic Functioning of Low-Relief, Deep Soil Watersheds and Hydrologic Legacies of Intensive Agriculture in the Calhoun Critical Zone Observatory, South Carolina, USA* (Doctoral dissertation, Duke University).

Norris, T. L., Gancarz, A. J., Rokop, D. J., & Thomas, K. W. (1983). Half-life of ^{26}Al. Journal of Geophysical Research: Solid Earth, 88(S01), B331-B333.

Lal, D. (1991). Cosmic ray labeling of erosion surfaces: in situ nuclide production rates and erosion models. Earth and Planetary Science Letters, 104(2-4), 424-439.

Marsh, G. P. (1882). *The earth as modified by human action: a new edition of man and nature*. Scribner's Sons.

Meade, R. H. (1982). Sources, sinks, and storage of river sediment in the Atlantic drainage of the United States. The Journal of Geology, 90(3), 235-252.

Meade, R. H., & Trimble, S. W. (1974). Changes in sediment loads in rivers of the Atlantic drainage of the United States since 1900. *International Association of Scientific Hydrology Publication*, *113*, 99-104.

Metz, L. J. (1958). *The Calhoun experimental forest*. US Department of Agriculture, Forest Service, Southeastern Forest Experiment Station.

Nishiizumi, K., Imamura, M., Caffee, M. W., Southon, J. R., Finkel, R. C., & McAninch, J. (2007). Absolute calibration of 10Be AMS standards. *Nuclear Instruments and Methods in Physics Research Section B: Beam Interactions with Materials and Atoms*, *258*(2), 403-413.

Phillips, J. D. (1992). The source of alluvium in large rivers of the lower Coastal Plain of North Carolina. *Catena*, *19*(1), 59-75.

Phillips, J. D., Marden, M., & Gomez, B. (2006). Residence time of alluvium in an aggrading fluvial system. *Earth Surface Processes and Landforms*, *32*(2), 307-316.

Richter, D. D., Eppes, M. C., Austin, J. C., Bacon, A. R., Billings, S. A., Brecheisen, Z., ... & Wade, A. M. (2020). Soil production and the soil geomorphology legacy of Grove Karl Gilbert. *Soil Science Society of America Journal*, *84*(1), 1-20.

Reusser, L., Bierman, P., & Rood, D. (2015). Quantifying human impacts on rates of erosion and sediment transport at a landscape scale. *Geology*, *43*(2), 171-174.

Schroeder, P. A., Austin, J. C., Thompson, A., & Richter, D. D. (2022). Mineralogical and Elemental Trends in Regolith on Historically Managed Sites in the southeastern United States Piedmont. *Clays and Clay Minerals*, *70*(4), 539-554.

Simmons, C. E. (1993). Sediment characteristics of North Carolina streams, 1970-79 (Vol. 2364). US Department of the Interior, US Geological Survey.

Soil Survey Staff, (2022). Natural Resources Conservation Service, United States Department of Agriculture. Web Soil Survey.

Steffen, W., Richardson, K., Rockström, J., Cornell, S. E., Fetzer, I., Bennett, E. M., & Sörlin, S. (2015). Planetary boundaries: Guiding human development on a changing planet. *Science*, *347*(6223), 1259855.

Stone, G. D. (1996). *Settlement ecology: The social and spatial organization of Kofyar agriculture*. University of Arizona Press.

Summerfield, M. A., & Hulton, N. J. (1994). Natural controls of fluvial denudation rates in major world drainage basins. Journal of Geophysical Research: Solid Earth, 99(B7), 13871-13883.

Syvitski, J. P., Vörösmarty, C. J., Kettner, A. J., & Green, P. (2005). Impact of humans on the flux of terrestrial sediment to the global coastal ocean. *science*, *308*(5720), 376-380.

Tarolli, P., Preti, F., & Romano, N. (2014). Terraced landscapes: From an old best practice to a potential hazard for soil degradation due to land abandonment. *Anthropocene*, *6*, 10-25.

Trimble, S. W. (1974). Man-induced soil erosion on the southern Piedmont. *Soil Conservation Society of America*.

Trimble, S. W. (1977). The fallacy of stream equilibrium in contemporary denudation studies. *American Journal of Science*, *277*(7), 876-887.

Trimble, S. W. (1985). Perspectives on the history of soil erosion control in the eastern United States. *Agricultural History*, *59*(2), 162-180.

Trimble, S. W. (2008). *Man-induced soil erosion on the Southern Piedmont, 1700-1970* (No. Ed. 2). Soil and Water Conservation Society.

US Department of Agriculture. (1940). Influences of vegetation and watershed treatment on runoff, silting, and stream flow. *US Dep. Agrie. Misc. Publ*, *397*, 1-80.

U.S. Geological Survey, 2016, The StreamStats program for South Carolina, online at http://water.usgs.gov/osw/streamstats/southcarolina.html, accessed on March 2, 2023.

U.S. Geological Survey, 2022, 3D Elevation Program – Hillshade Stretched: U.S. Geological Survey. Accessed December 9, 2022.

U.S. Geological Survey, 2022, 3D Elevation Program 10-Meter 1/3 Arc Second Resolution: U.S. Geological Survey. Accessed April 1, 2022.

von Blanckenburg, F., Hewawasam, T., & Kubik, P. W. (2004). Cosmogenic nuclide evidence for low weathering and denudation in the wet, tropical highlands of Sri Lanka. *Journal of Geophysical Research: Earth Surface*, *109*(F3).

Wade, A. M., Richter, D. D., Cherkinsky, A., Craft, C. B., & Heine, P. R. (2020). Limited carbon contents of centuries old soils forming in legacy sediment. *Geomorphology*, *354*, 107018.

Walling, D. E. (1983). The sediment delivery problem. *Journal of hydrology*, 65(1-3), 209-237.

Walter, R. C., & Merritts, D. J. (2008). Natural streams and the legacy of water-powered mills. *Science*, 319(5861), 299-304.

Wells, N. A., & Andriamihaja, B. (1993). The initiation and growth of gullies in Madagascar: are humans to blame?. *Geomorphology*, *8*(1), 1-46.

Whipple, K. X., Wobus, C., Crosby, B., Kirby, E., & Sheehan, D. (2007). New tools for quantitative geomorphology: Extraction and interpretation of stream profiles from digital topographic data. GSA short course, 506, 1-26.

Wilkinson, B. H., & McElroy, B. J. (2007). The impact of humans on continental erosion and sedimentation. Geological Society of America bulletin, 119(1-2), 140-156.

Willett, S. D., & Brandon, M. T. (2002). On steady states in mountain belts. *Geology*, *30*(2), 175-178.

Wilkinson, B. H., & McElroy, B. J. (2007). The impact of humans on continental erosion and sedimentation. *GeologicalSsociety of America bulletin*, *119*(1-2), 140-156.

Zonneveld, I. S. (1989). The land unit—a fundamental concept in landscape ecology, and its applications. *Landscape ecology*, *3*, 67-86.

Table 1: CRONUS input values to calculate the basin-wide average denudation rate (version: 3.0, muons: 3) (http://hess.washington.edu).

Sample name	Latitude	Longitude	Elevation	Elv/pressure	Thickness	Density	Shielding	[Be-10]	+/-	Be	[Al-26]	+/-	Al
ID	(DD)	(DD)	(m)	flag	(cm)	(g/cm^3)	correction	$atoms/g^{-1}$	$atoms/g^{-1}$	standardization	$atoms\ g^{-1}$	$atoms\ g^{-1}$	standardization
CCZO-002	34.61	-81.699	154.012	std	0.1	2.65	1	341480.6376	7405.74966	07KNSTD	0	0	KNSTD
CCZO-003	34.609	-81.701	157.765	std	0.1	2.65	1	340249.1772	7367.05263	07KNSTD	0	0	KNSTD
CCZO-004	34.607	-81.703	161.733	std	0.1	2.65	1	346897.6103	7553.15211	07KNSTD	0	0	KNSTD
CCZO-005	34.606	-81.705	164.285	std	0.1	2.65	1	361328.6919	7255.30848	07KNSTD	0	0	KNSTD
CCZO-006	34.604	-81.708	169.051	std	0.1	2.65	1	461670.2161	8554.06994	07KNSTD	0	0	KNSTD
CCZO-007	34.89	-82.079	243.878	std	0.1	2.65	1	348298.9878	16589.63319	07KNSTD	0	0	KNSTD
CCZO-008	34.901	-82.095	244.559	std	0.1	2.65	1	375349.4833	7737.96788	07KNSTD	0	0	KNSTD

Table 2 The ^{10}Be concentrations and calculated denudation rates with uncertainties are display here. The ^{10}Be concentrations in the seventh column were calculated by determining the amount of ^{9}Be present, multiplying that value by the normalized background corrected ratio, and then dividing by the quartz mass. The denudation rates were determined using the CRONOUS online calculator and the statistics derived form the delineated watershed.

Sample ID	Quartz Mass (g)	Uncorrected ^{10}Be/^{9}Be Ratio	Uncorrected ^{10}Be/^{9}Be Ratio Uncertainty	Background Corrected ^{10}Be/^{9}Be Ratio	Background Corrected ^{10}Be/^{9}Be Ratio Uncertainty	^{10}Be Concentration (atoms/g^{-1})	^{10}Be Concentration Uncertainty (atoms/g^{-1})
CZ21-002	21.9025	4.507E^{-15}	9.574E^{-15}	4.460E^{-13}	9.673E^{-15}	3.415E^{+5}	7.406E^{+3}
CZ21-003	21.7971	4.460E^{-15}	9.455E^{-15}	4.413E^{-13}	9.556E^{-15}	3.402E^{+5}	7.367E^{+3}
CZ21-004	20.7990	4.324E^{-15}	9.212E^{-15}	4.278E^{-13}	9.315E^{-15}	3.469E^{+5}	7.553E^{+3}
CZ21-005	21.6471	4.740E^{-15}	9.323E^{-15}	4.694E^{-13}	9.425E^{-15}	3.613E^{+5}	7.255E^{+3}
CZ21-006	21.8468	6.011E^{-15}	1.097E^{-14}	5.965E^{-13}	1.105E^{-14}	4.617E^{+5}	8.554E^{+3}
CZ21-007	4.1948	9.152E^{-15}	3.901E^{-15}	8.689E^{-14}	4.139E^{-15}	3.483E^{+5}	1.659E^{+4}
CZ21-008	21.8711	4.926E^{-15}	9.965E^{-15}	4.880E^{-13}	1.006E^{-14}	3.753E^{+5}	7.738E^{+3}

Table 3. ^{26}Al and ^{10}Be concentrations and ratios for the soil pit samples, which were measured on an accelerated mass spectrometer at Purdue University Prime Laboratory.

Sample Name	Quartz Mass (g)	^{26}Al Concentration (atoms g^{-1})	^{26}Al Concentration Uncertainty (atoms g^{-1})	^{10}Be Concentration (atoms g^{-1})	^{10}Be Concentration Uncertainty (atoms g^{-1})	$^{26}Al/^{10}Be$ Ratio	$^{26}Al/^{10}Be$ Ratio Uncertainty
R1C2-01+02	22.06	1.960E+06	7.839E+04	4.157E+05	8.763E+03	4.71	0.21
R1C2-03+04	10.02	4.405E+05	2.442E+04	8.123E+04	6.312E+03	5.42	0.52
R1C2-05+06	22.15	1.906E+05	1.486E+04	4.095E+04	2.846E+03	4.65	0.49
R1C3-01	22.32	3.504E+06	1.280E+05	6.682E+05	1.340E+04	5.24	0.22
R1C3-02	18.69	2.450E+06	8.165E+04	4.221E+05	1.417E+04	5.80	0.27
R1C3-03	8.22	9.854E+05	4.892E+04	1.696E+05	9.655E+03	5.81	0.44
R1C3-04	9.51	2.616E+05	2.032E+04	3.923E+04	4.677E+03	6.67	0.95
R2H1-06	17.10	1.444E+05	1.189E+04	2.037E+04	2.593E+03	7.09	1.07
R7H2-06	14.33	3.055E+06	9.832E+04	4.501E+05	1.118E+04	6.79	0.28
R7P2-08	16.13	1.924E+05	1.342E+04	3.021E+04	4.491E+03	6.37	1.05
R8H1-01	5.96	2.125E+06	8.485E+04	2.993E+05	1.668E+04	7.10	0.49
R8H1-02	5.38	6.587E+05	4.403E+04	1.042E+05	9.698E+03	6.32	0.72
R8H1-03+04	10.72	2.035E+05	2.252E+04	2.705E+04	3.977E+03	7.52	1.38

Table 4: Comparing *in situ*-produced ^{10}Be derived erosion rates for six of the ten basins studied by Reusser et al. (2015) and Trimble (1977) to the Broad River Basin measurements. The Broad River Basin is the basin researched in this paper, showing a similar denudation rate to the Oconee Basin and Roanoke Basin.

Basin	Sample Type	^{10}Be Concentrations (atoms/g x 10^5)	Denudation Rates (m/My)
Roanoke	Mid-basin	6.35 ± 0.18	6.36 ± 0.54
Neuse	Mid-basin	9.79 ± 0.25	3.11 ± 0.28
Saluda	Mid-basin	3.65 ± 0.09	11.01 ± 0.85
Savannah	Mid-basin	2.81 ± 0.08	15.62 ± 1.19
Oconee	Mid-basin	4.83 ± 0.12	7.13 ± 0.59
Chattahoochee	Mid-basin	3.29 ± 0.08	12.44 ± 0.95
Broad	Mid-basin	3.67 ± 0.08	7.11 ± 0.19

Table 5. Sediment yield data (1970-79) from Simmons (1993) based on North Carolina tributary's in the Blue Ridge (B), Piedmont (P), and Coastal Plain (C) physiographic provinces for forested, forested with minor development, and rural agriculture lands, with calculated long-term sediment yield (m/Ma). Holcombe's Branch sediment yield and long-term yield was derived from the Watershed Erosion Prediction Project.

Tributary	Providence	Land Cover	Drainage Area (km^2)	Estimated mean long-term suspended sediment yield (m/Ma)
Holcombe's Branch	P	Agriculture and then reforested	6.1	161.5
Black Swamp	C	Forested	2.6	1.4
Cane Creek	P	Forested	1.7	11.0
Ellis Creek	C	Forested	4.7	1.2
Dutchman’s creek	P	Forested	8.9	9.6
Beetree Creek	B	Forested	14.1	7.2
Cataloochee Creek	B	Forested	127.4	10.0
Nantahala River	B	Forested	134.4	13.5
Buckhorn Creek	B	Forested with minor development	197.6	17.7
Flat Creek	C	Forested with minor development	19.8	14.0
Linville River	B	Forested with minor development	172.8	25.7
Jacob Fork	P	Forested with minor development	66.6	65.4

Table 5 continued. Sediment yield data (1970-79) from Simmons (1993) based on North Carolina tributary's in the Blue Ridge (B), Piedmont (P), and Coastal Plain (C) physiographic provinces for forested, forested with minor development, and rural agriculture lands, with calculated long-term sediment yield (m/Ma). Holcombe's Branch sediment yield and long-term yield was derived from the Watershed Erosion Prediction Project.

Tributary	Providence	Land Cover	Drainage Area (km^2)	Estimated mean long-term suspended sediment yield (m/Ma)
Davidson River	B	Forested with minor development	104.6	14.0
West Fork Pigeon	B	Forested with minor development	71.5	49.0
South Toe River	B	Forested with minor development	112.1	30.4
Dan River near Francisco	P	Rural agriculture	334.1	63.0
Dan River near Wentworth	P	Rural agriculture	2727.3	102.7
Hyco Creek	P	Rural agriculture	118.9	39.7
Double Creek	P	Rural agriculture	19.3	95.7
South Hyco Creek	P	Rural agriculture	146.3	42.0
Tar River near TR	P	Rural agriculture	432.5	16.3
Tar River near Louisburg	P	Rural agriculture	1105.9	23.4

Table 5 continued. Sediment yield data (1970-79) from Simmons (1993) based on North Carolina tributary's in the Blue Ridge (B), Piedmont (P), and Coastal Plain (C) physiographic provinces for forested, forested with minor development, and rural agriculture lands, with calculated long-term sediment yield (m/Ma). Holcombe's Branch sediment yield and long-term yield was derived from the Watershed Erosion Prediction Project.

Tributary	Providence	Land Cover	Drainage Area (km^2)	Estimated mean long-term suspended sediment yield (m/Ma)
Cedar Creek	P	Rural agriculture	124.8	19.6
Swift Creek	P	Rural agriculture	429.9	22.4
Little Fishing Creek	C	Rural agriculture	458.4	9.8
Tar River near Tarboro	C	Rural agriculture	1362.3	10.0
Chicod Creek	C	Rural agriculture	5654.0	10.3
Durham Creek	C	Rural agriculture	116.6	2.8
Eno River near Hillsborough	P	Rural agriculture	67.3	39.7
Eno River near Durham	P	Rural agriculture	170.9	37.4
Little River	P	Rural agriculture	208.2	32.7
Flat River	P	Rural agriculture	385.9	44.4
Neuse River	P	Rural agriculture	1385.7	32.7

Table 5 continued. Sediment yield data (1970-79) from Simmons (1993) based on North Carolina tributary's in the Blue Ridge (B), Piedmont (P), and Coastal Plain (C) physiographic provinces for forested, forested with minor development, and rural agriculture lands, with calculated long-term sediment yield (m/Ma). Holcombe's Branch sediment yield and long-term yield was derived from the Watershed Erosion Prediction Project.

Tributary	Providence	Land Cover	Drainage Area (km^2)	Estimated mean long-term suspended sediment yield (m/Ma)
Middle Creek	P	Rural agriculture	216.3	12.6
Little River near Kenly	C	Rural agriculture	494.7	9.8
Little River near Princeton	C	Rural agriculture	600.9	10.0
Bear creek	C	Rural agriculture	11.1	5.4
Turner Swamp	C	Rural agriculture	5.4	10.5
Contentnea Creek	C	Rural agriculture	1888.1	6.3
Little Contentnea Creek	C	Rural agriculture	241.6	8.2
Creeping Swamp near Calico	C	Rural agriculture	25.4	6.8
Creeping Swamp near Vanceboro	C	Rural agriculture	69.9	7.9
Palmetto Swamp	C	Rural agriculture	62.7	9.6

Table 5 continued. Sediment yield data (1970-79) from Simmons (1993) based on North Carolina tributary's in the Blue Ridge (B), Piedmont (P), and Coastal Plain (C) physiographic provinces for forested, forested with minor development, and rural agriculture lands, with calculated long-term sediment yield (m/Ma). Holcombe's Branch sediment yield and long-term yield was derived from the Watershed Erosion Prediction Project.

Tributary	Providence	Land Cover	Drainage Area (km^2)	Estimated mean long-term suspended sediment yield (m/Ma)
Trent River near Trenton	C	Rural agriculture	435.1	2.6
Reedy Fork	P	Rural agriculture	53.4	58.4
Big Alamanace Creek	P	Rural agriculture	300.4	46.7
Cane Creek near	P	Rural agriculture	87.3	35.0
Haw River	P	Rural agriculture	3307.4	32.7
New Hope near Pittsboro	P	Rural agriculture	745.9	18.7
Deep River near Randleman	P	Rural agriculture	323.8	49.0

Soil Map of Holcombe's Branch, Union County, South Carolina

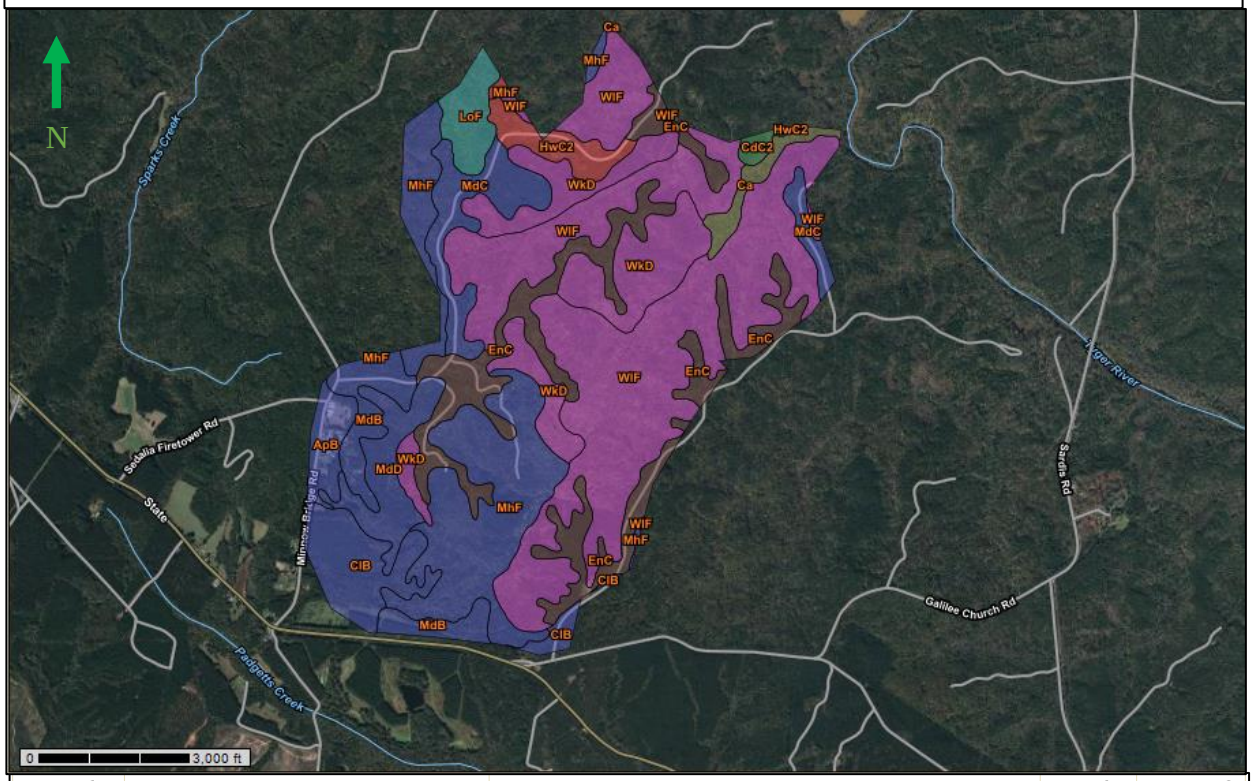

Map unit symbol	Map unit name	Rating	Acres in AOI	Percent of AOI
ApB	Appling loamy sand, 2 to 6 percent slopes	residuum weathered from gneiss and/or residuum weathered from granite	34.3	1.9%
Ca	Cartecay-Toccoa complex	loamy alluvium	24.9	1.4%
CdC2	Cataula sandy loam, 6 to 10 percent slopes, eroded	clayey residuum weathered from granite and gneiss	8.4	0.5%
ClB	Cecil sandy loam, 2 to 6 percent slopes	residuum weathered from gneiss and/or granite	93.9	5.3%
EnC	Enon sandy loam, 6 to 10 percent slopes	clayey residuum weathered from schist and gneiss with intrusions of diorite or hornblende	228.5	12.9%
HwC2	Hiwassee sandy loam, 6 to 10 percent slopes, eroded	clayey residuum weathered from gneiss or schist	40.0	2.3%
HyC2	Hiwassee sandy clay loam, 6 to 10 percent slopes, eroded	clayey residuum weathered from gneiss or schist	2.2	0.1%
LoF	Louisburg loamy sand, 10 to 40 percent slopes	clayey residuum weathered from granite and gneiss	41.9	2.4%
MdB	Madison sandy loam, 2 to 6 percent slopes	clayey residuum weathered from granite and gneiss	73.5	4.1%
MdC	Madison sandy loam, 6 to 10 percent slopes	clayey residuum weathered from granite and gneiss	96.7	5.4%
MdD	Madison sandy loam, 10 to 15 percent slopes	clayey residuum weathered from granite and gneiss	69.1	3.9%
MhF	Madison and Pacolet soils, 15 to 40 percent slopes	clayey residuum weathered from granite and gneiss	266.9	15.0%
WkD	Wilkes sandy loam, 6 to 15 percent slopes	clayey residuum weathered from hornblende gneiss or diorite	191.1	10.8%
WlF	Wilkes soils, 15 to 40 percent slopes	clayey residuum weathered from hornblende gneiss or diorite	603.7	34.0%
Totals for Area of Interest			**1,775.1**	**100.0%**

Fig 4: Soil Map of Holcombe's Branch, Union County, South Carolina with the listed soil types (Soil Survey Staff, 2022).

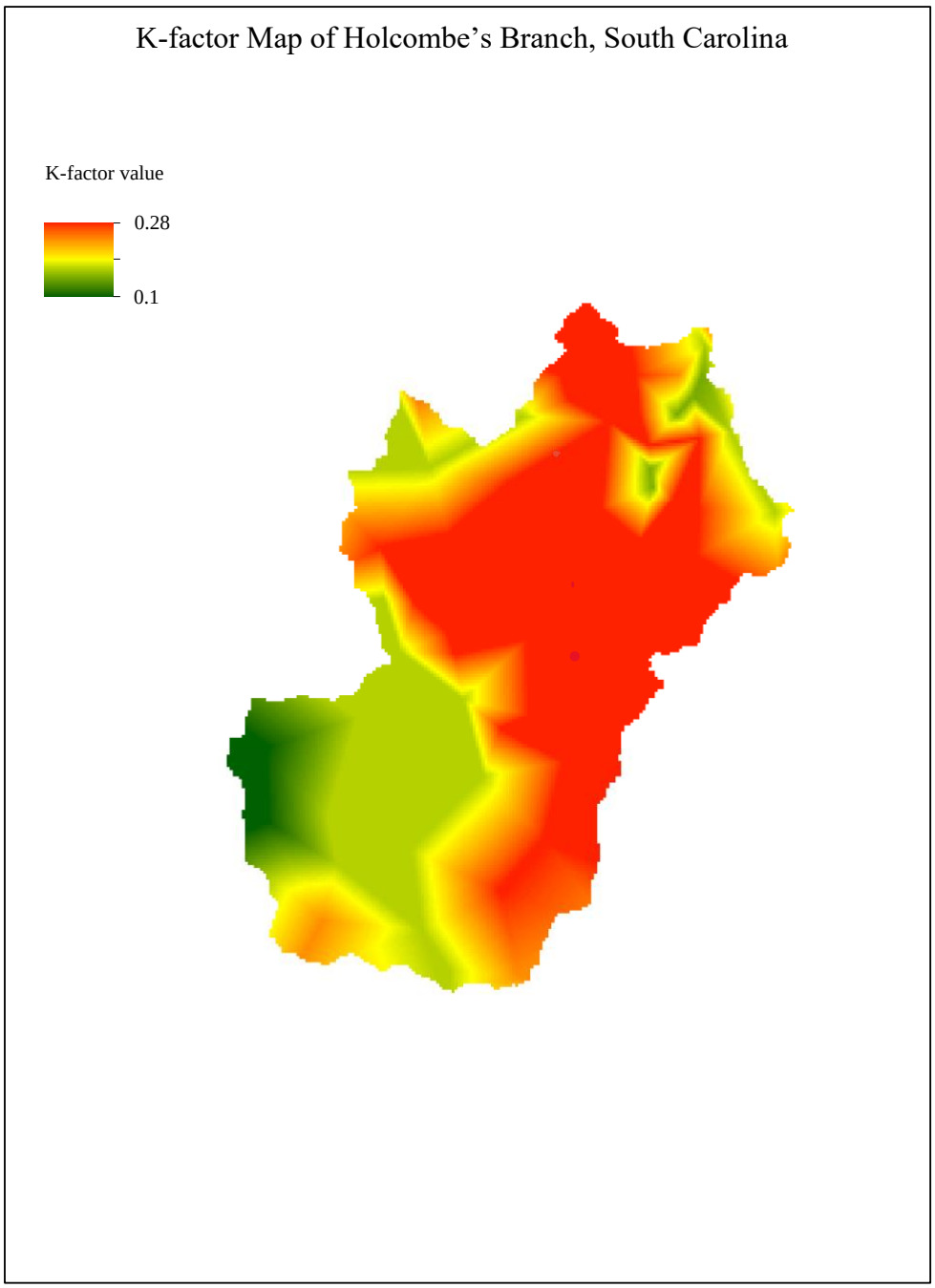

Fig. 5: The K-Factor map, created in ArcMap, showing how susceptible the soil in Holcombe's Branch is to erosion (Soil Survey Staff, 2022).

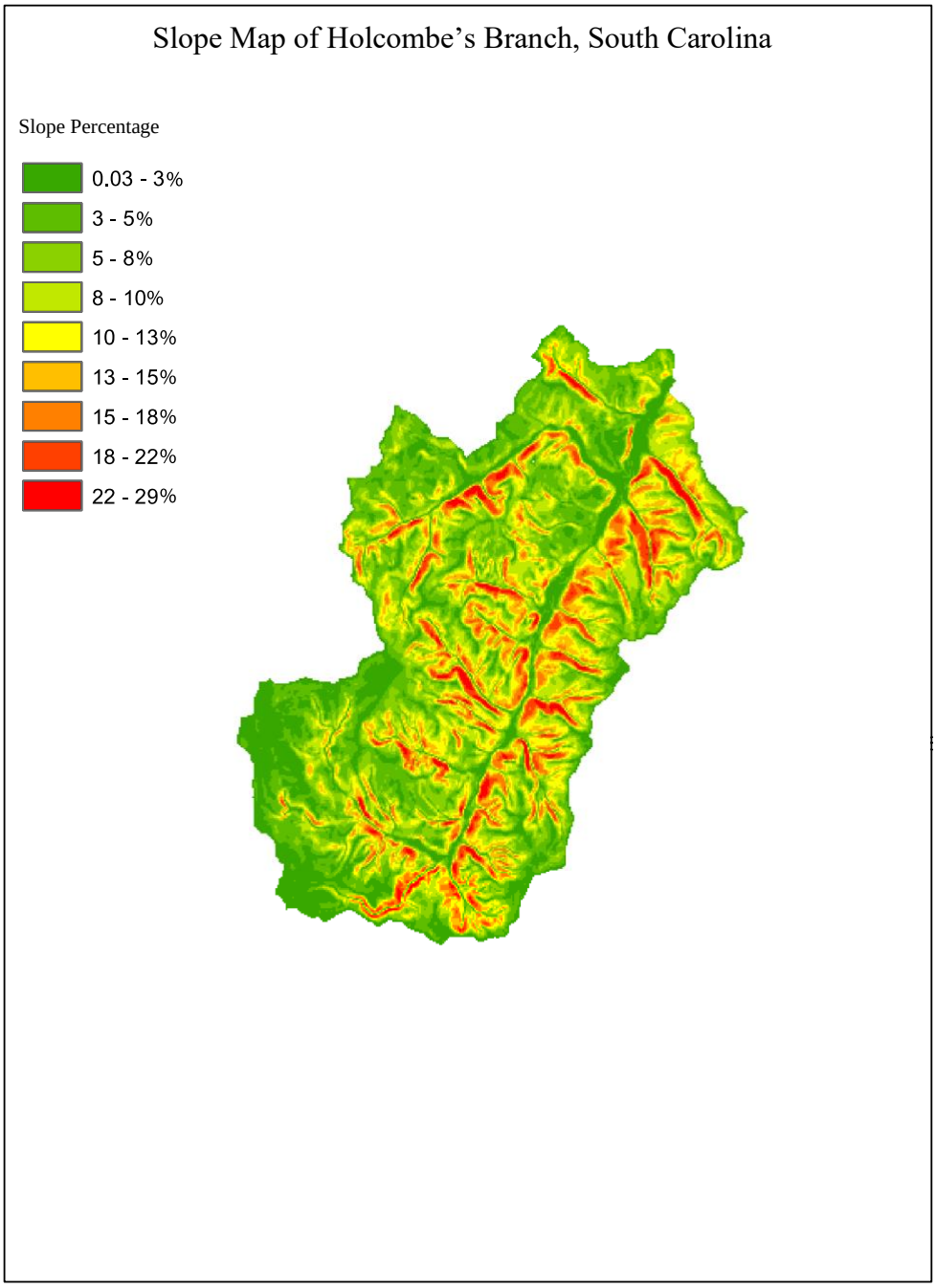

Fig. 6: The slope map, created in ArcMap, depicting the percentage slopes in Holcombe's Branch, Union County, South Carolina.

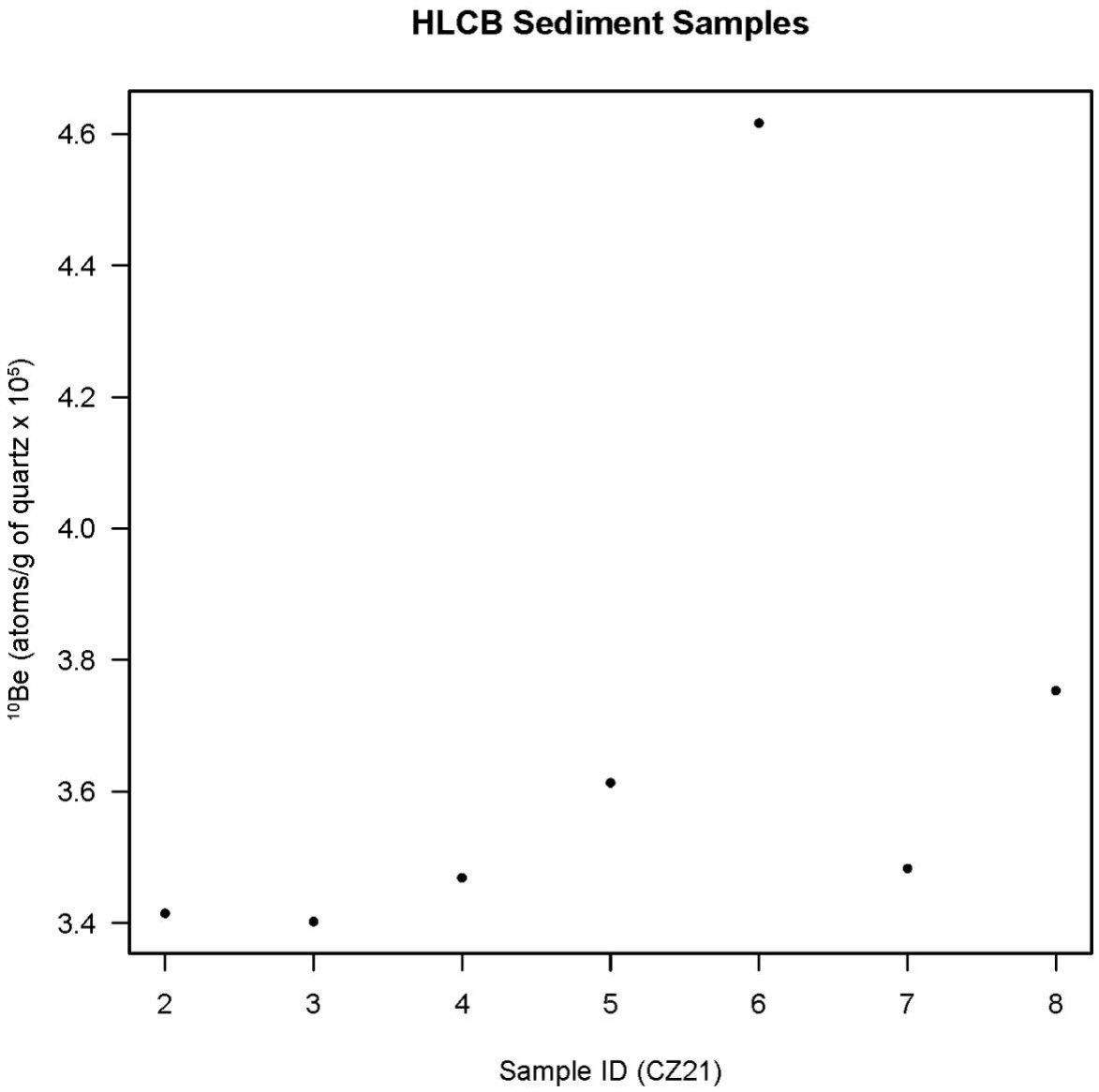

Fig. 7: Holcombe's Branch fluvial sediment samples showing the ^{10}Be cosmogenic nuclide concentrations. From sample ID 2 (CZ21-002) at the mouth of HLCB stream to 6 at the headwater (CZ21-006). Sample ID 7 (CZ21-007) is downstream Tyger River and 8 (CZ21-008) is upstream Tyger River.

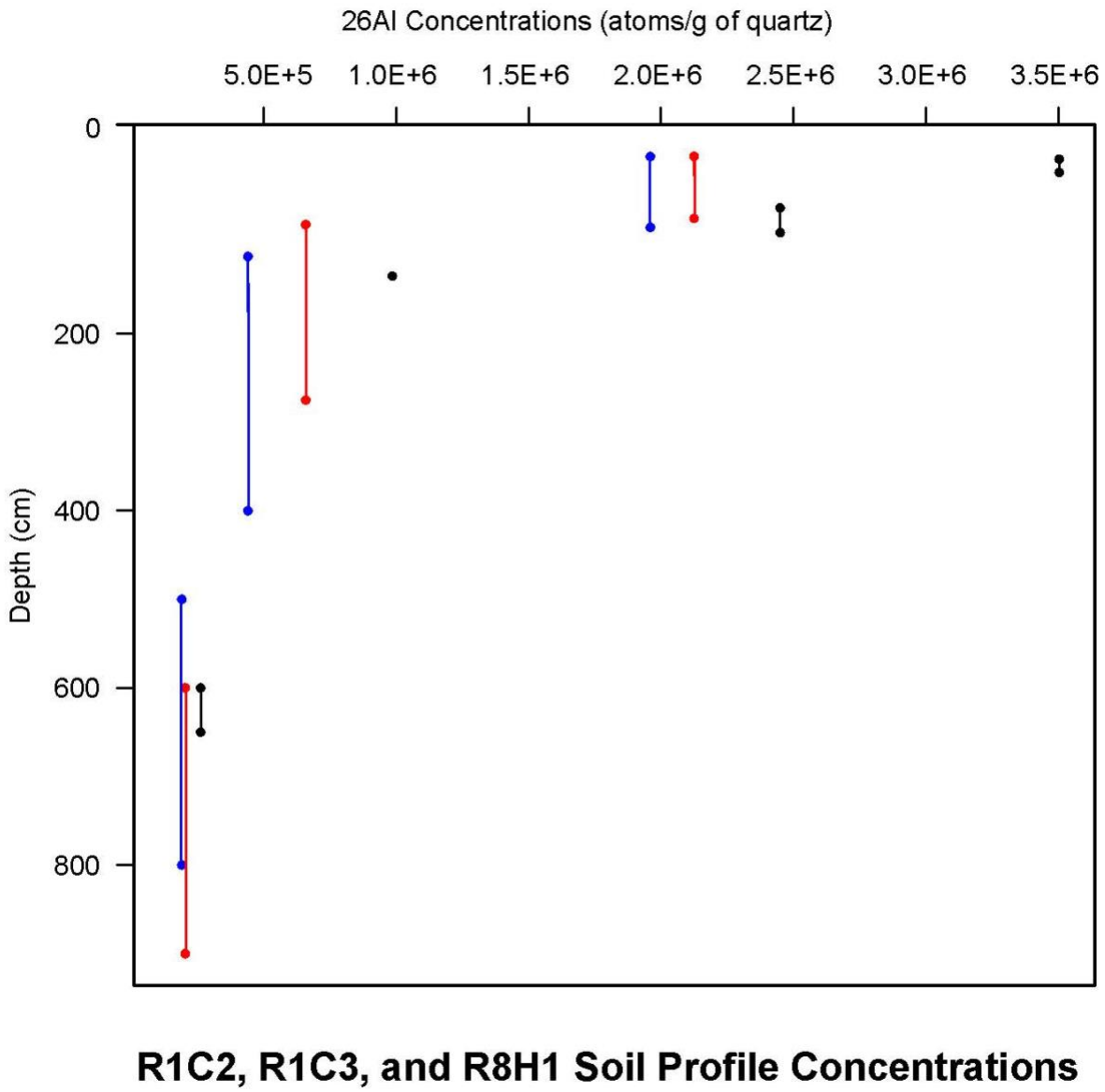

Fig. 8: Soil Pit 26Al concentrations for R1C2 (blue), R1C3 (black), R8H1 (red), showing that the production of cosmogenic concentrations has a non-linear relationship to depth (Granger et al., 2013).

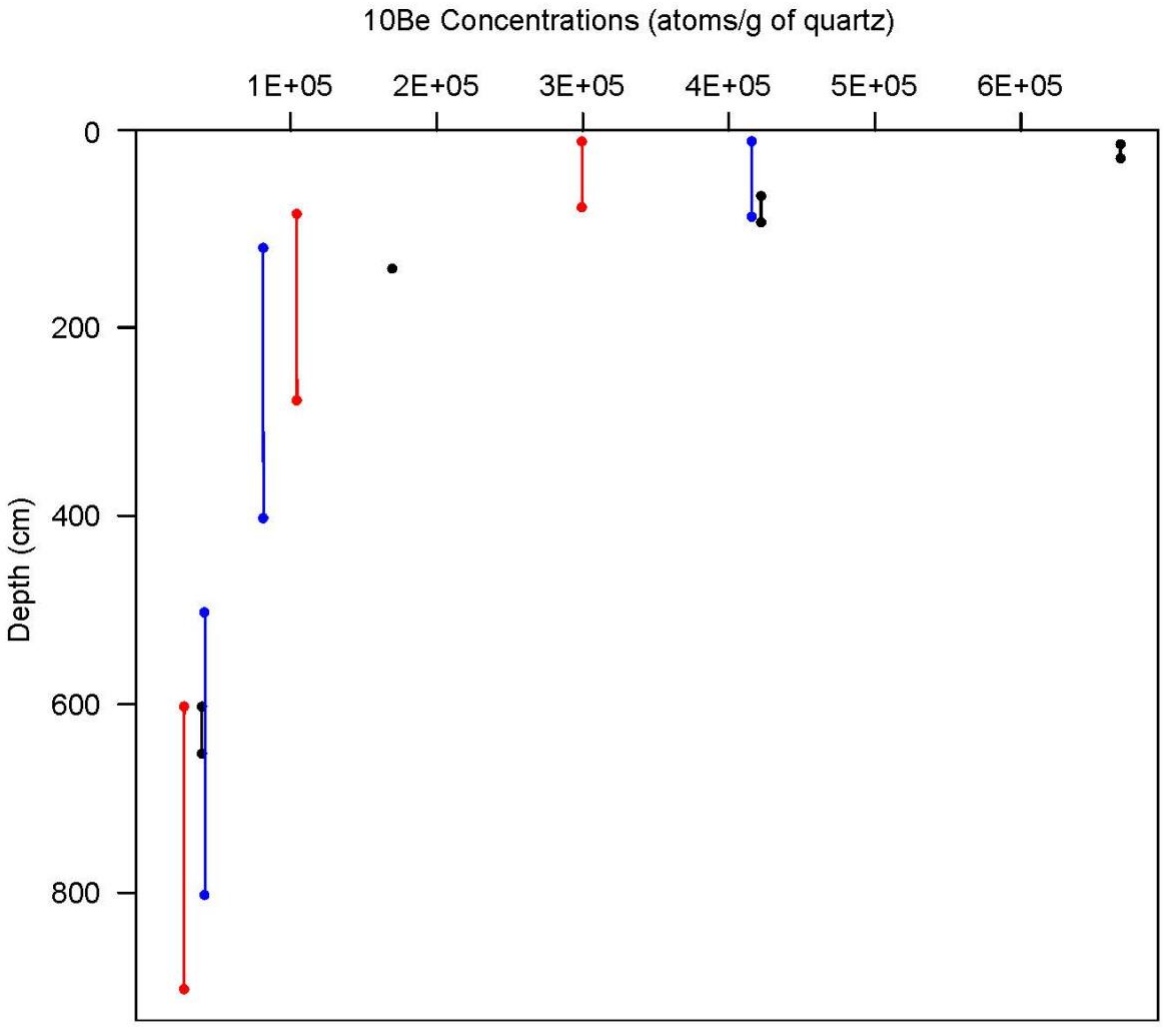

Fig. 9: Soil Pit ^{10}Be concentrations for R1C2 (blue), R1C3 (black), and R8H1(red), showing that the production of cosmogenic concentrations is non-linear relationship to depth (Granger et al., 2013).

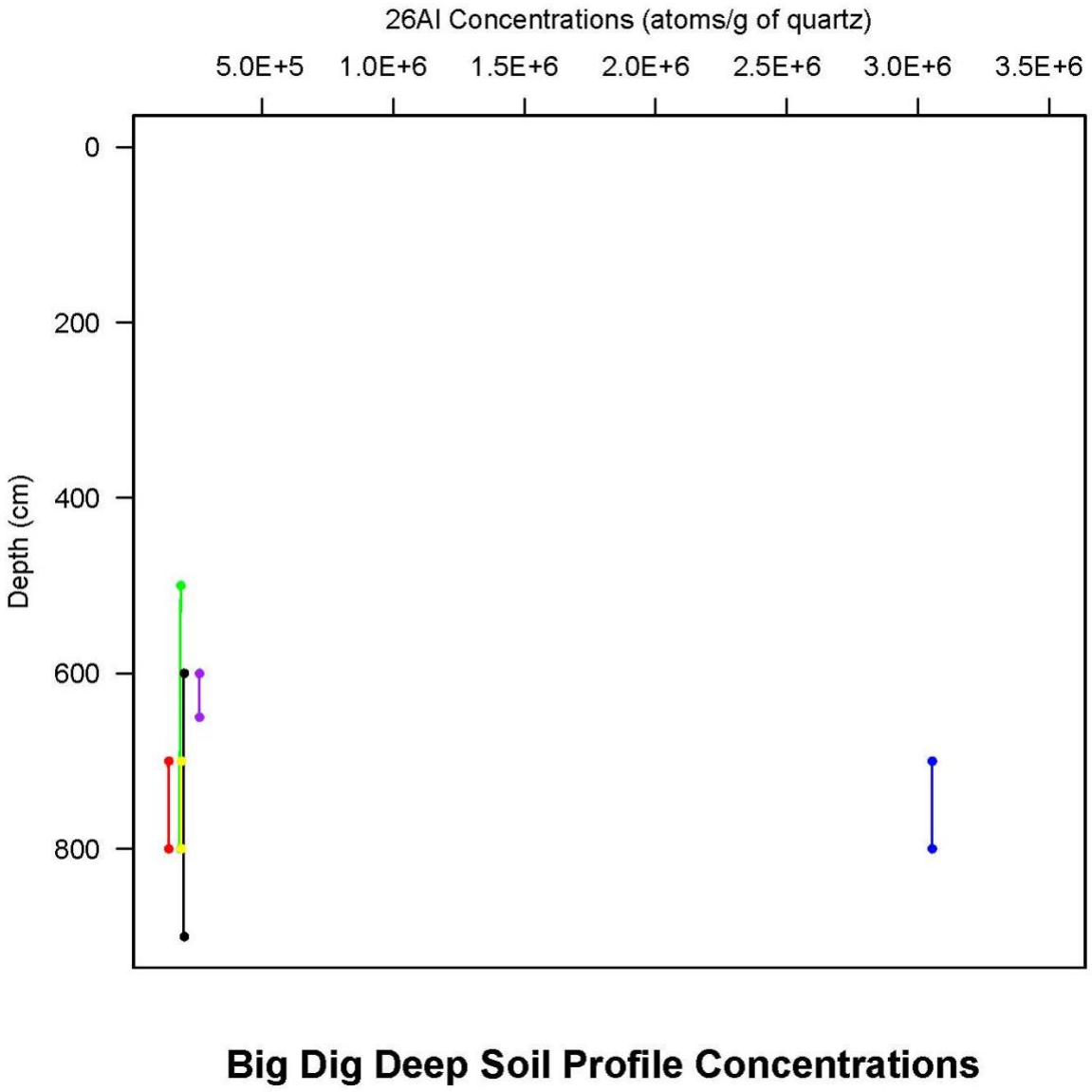

Fig. 10: Soil Pit 26Al concentrations for R1C2 (green), R1C3 (purple), R8H1 (black), R2H1 (red), R7P2 (yellow), R7H2 (blue) showing the production of cosmogenic concentrations, mainly from muon penetrations are low at depths of 500 plus centimeters (Granger et al., 2013; Schroeder et al., 2022).

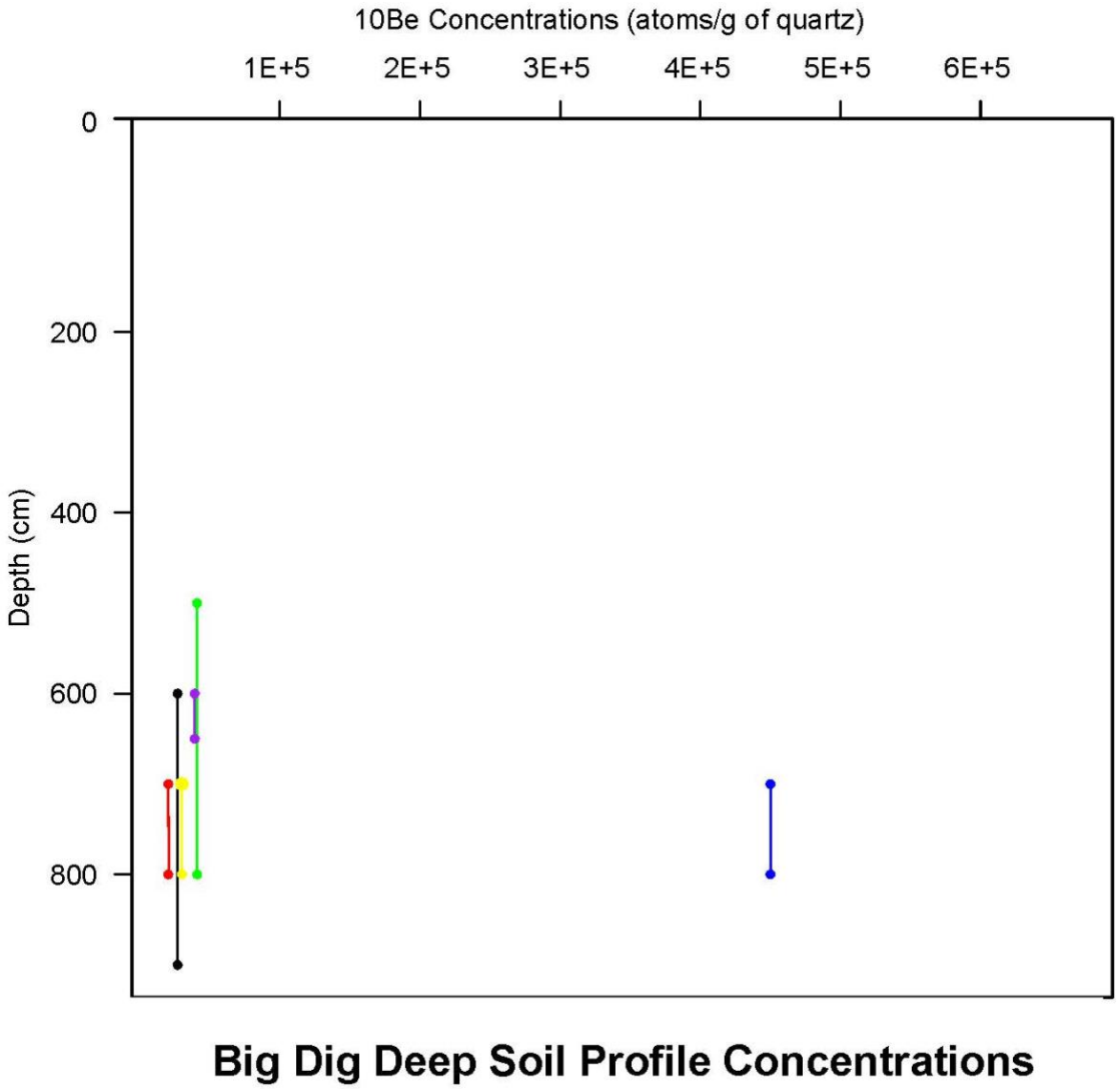

Fig. 11. Soil Pit ^{10}Be concentrations for R1C2 (green), R1C3 (purple), R8H1 (black), R2H1 (red), R7P2 (yellow), R7H2 (blue) showing the production of cosmogenic concentrations, mainly from muon penetrations are low at depths of 500 plus centimeters (Granger et al., 2013; Schroeder et al., 2022).

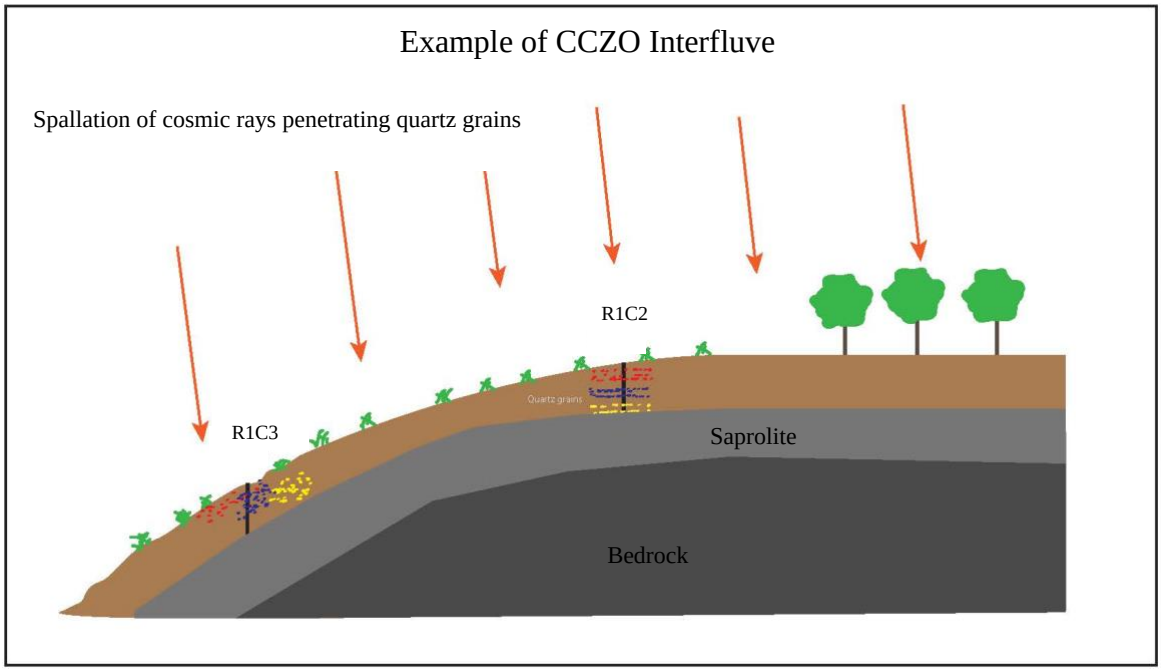

Fig. 12. The interfluve example represents the position of soil pits R1C2 and R1C3. R1C2 should have a higher concentration of cosmogenic nuclides than R1C3, due to less mobilized soil higher up on the interfluve. That is not the case here. R1C2 has a lower concentration of cosmogenic nuclides, suggesting that anthropogenic influence may have brought quartz grains with smaller concentrations of cosmogenic nuclides towards the surface.

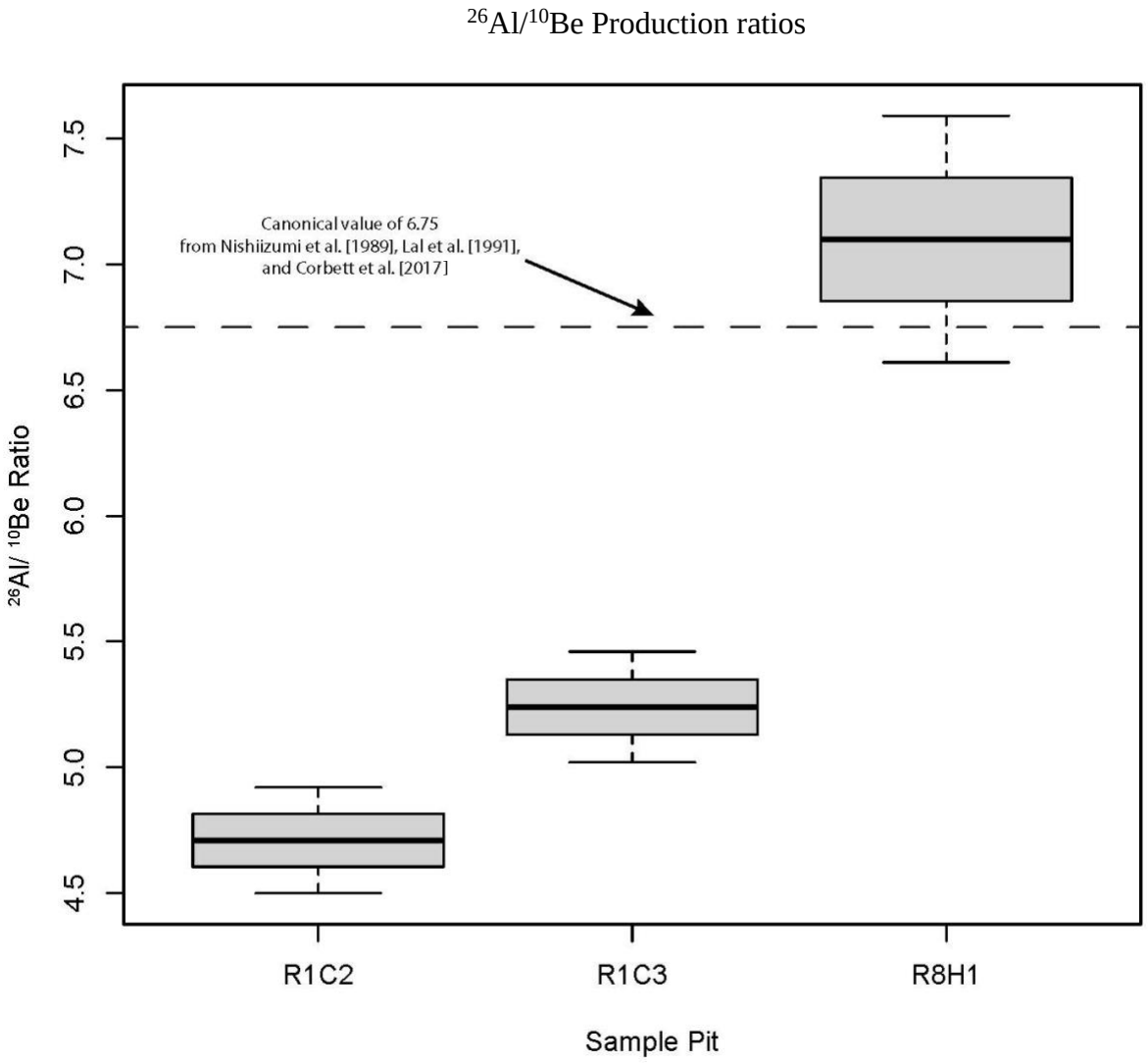

Fig. 13. ^{26}Al/^{10}Be ratios for soil pits R1C2, R1C3, and R8H1. The dotted line represents the canonical value determined from Lal et al. (1991), Nishizumi (2007), and Chmeleff et al. (2010).

LiDAR Imaging of Legacy Sediments in Holcombe's Branch, Union, South Carolina

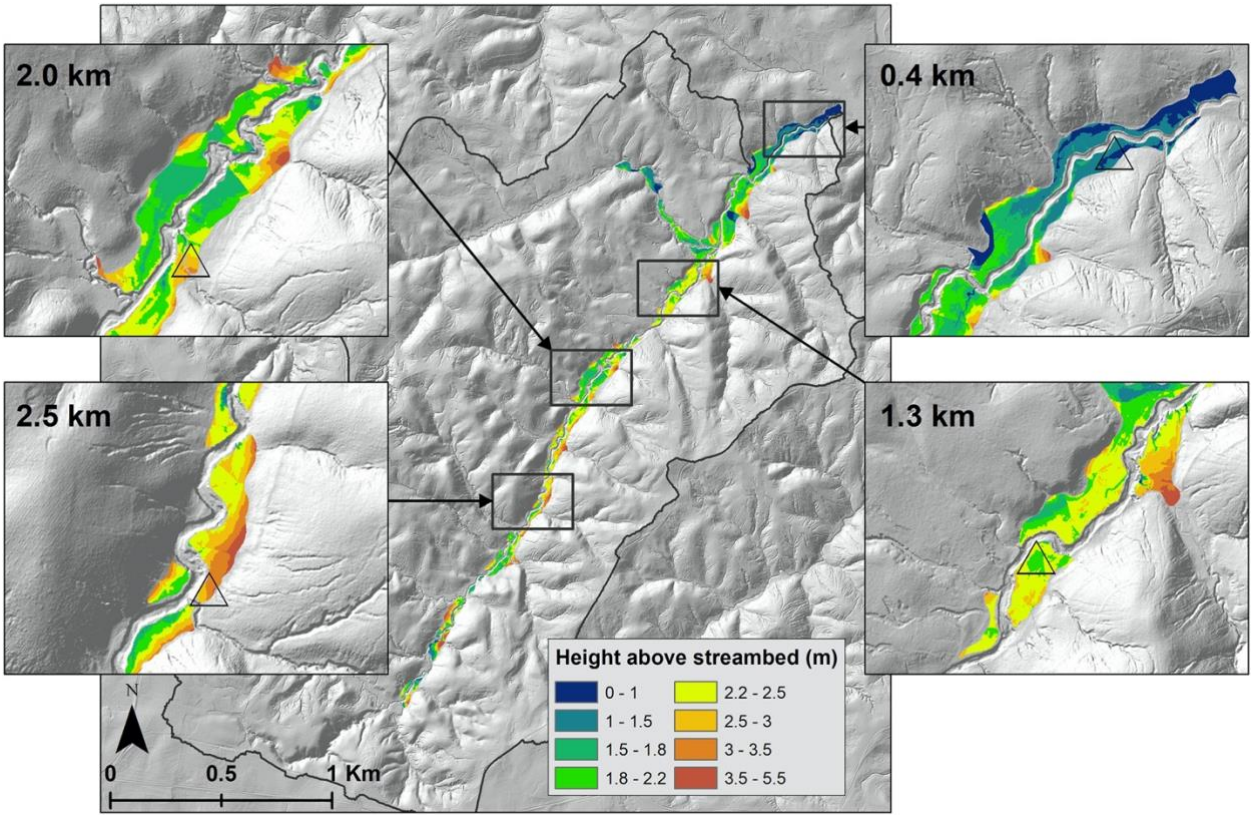

Fig. 14. LiDAR-derived 1m^2 DEM showing the floodplain height within Holcombe's Branch (Wade et al., 2020). The flood plain height above the stream channel is presented by the colors (Wade et al., 2020). The inset images reflect individual distances upstream showing floodplain height, and the triangles indicate locations of vegetation plots described in Wade et al. (2020).

Appendices APPENDIX A

Mean Sediment Yields for North Carolina Physiographic Provinces

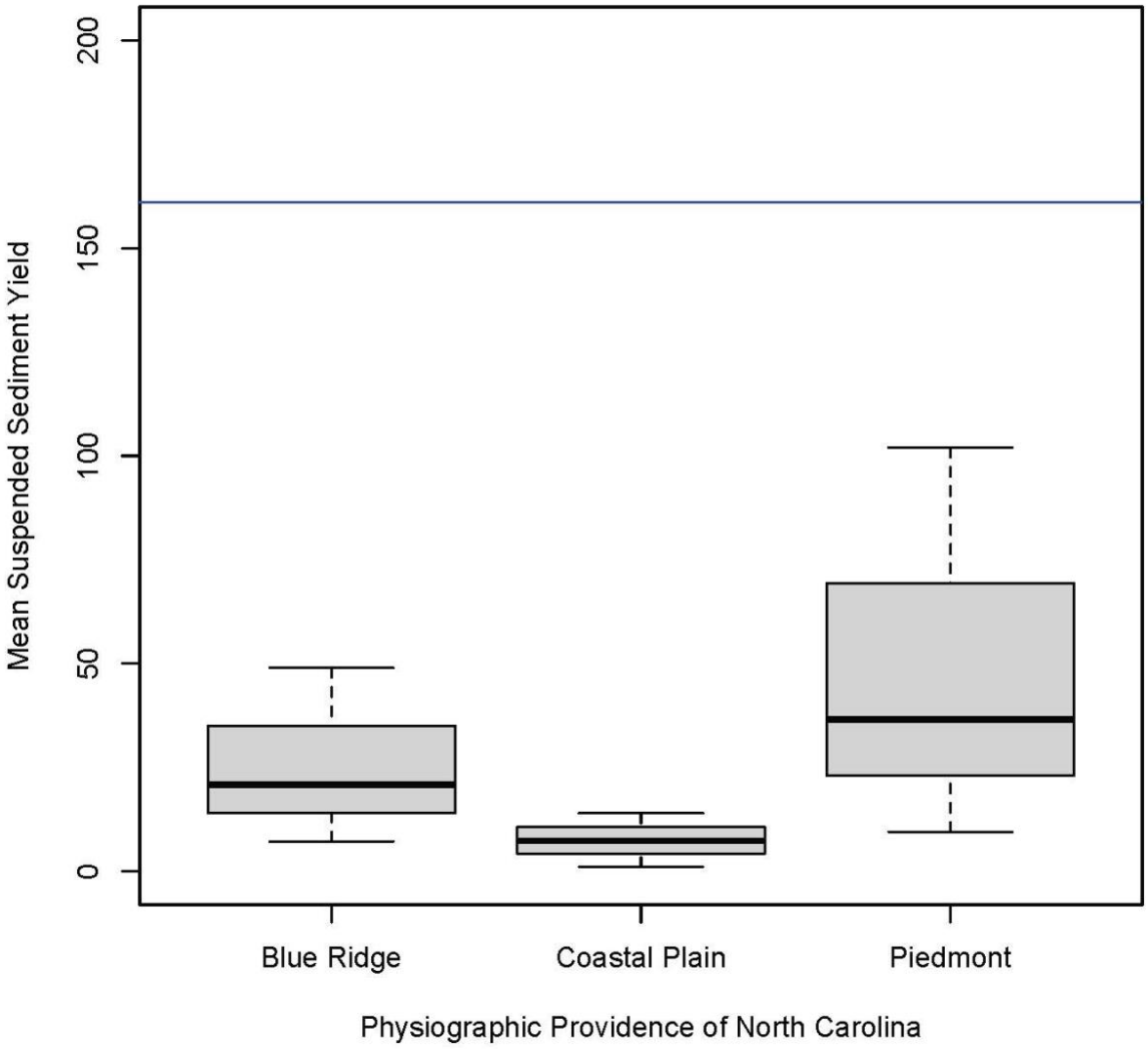

A. The boxplot of North Carolina physiographic province's plots the mean sediment yield for forested, forested with minor development, and/or rural agricultural land (Simmons, 1993). The Blue Ridge: mean = 20.9 m/Ma, lower (Simmons, 1993), providing a lower, long-term, sediment yield than the long-term sediment yield for Holcombe's Branch, 161.5 m/Ma (blue horizontal line). The Piedmont: mean = 36.6 m/Ma. The Coastal Plain: mean = 74 m/Ma.

APPENDIX B

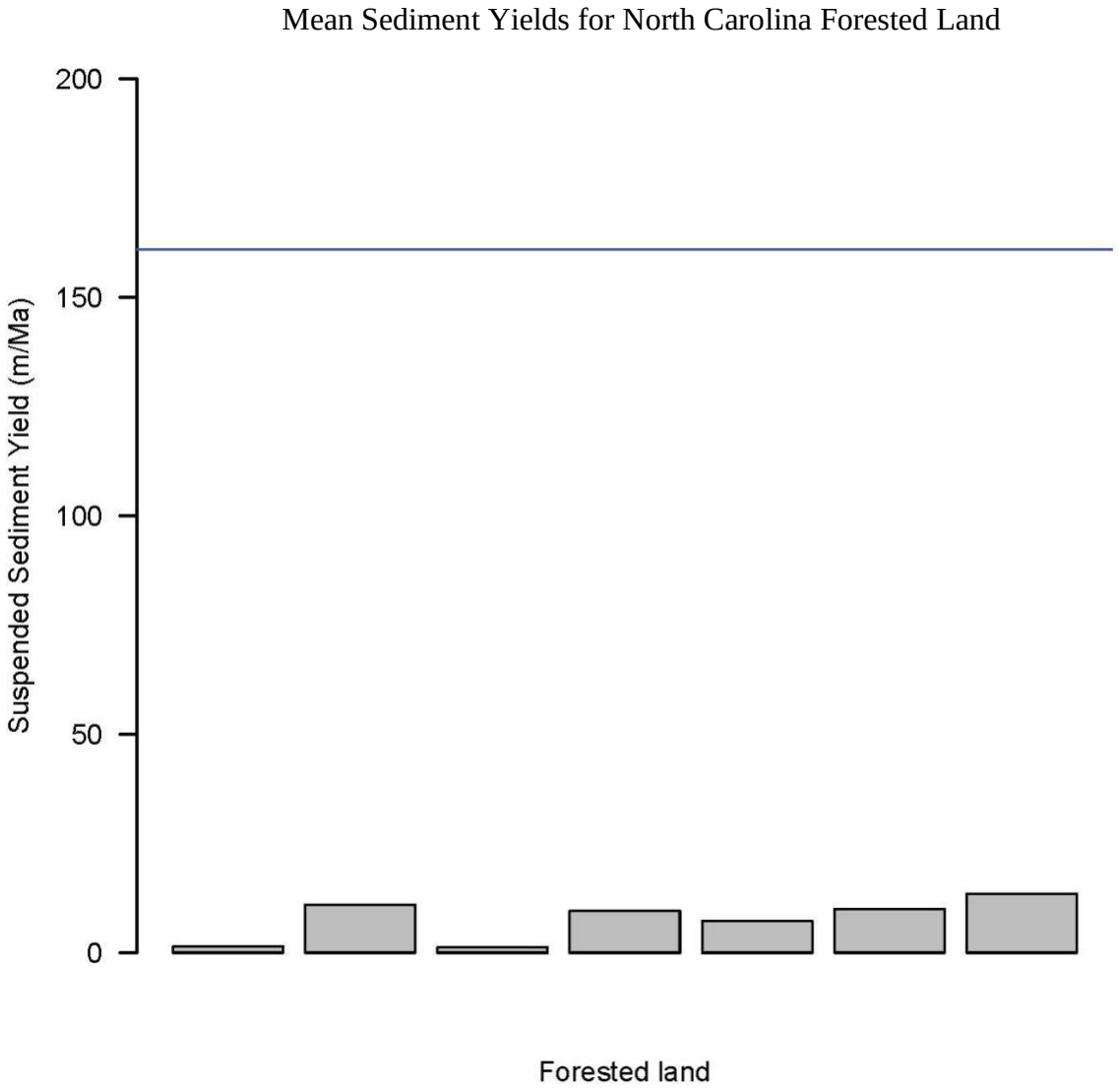

B. The bar plot shows the long-term sediment yields of North Carolina tributaries in forested regions (Simmons, 1993). The blue line represents Holcombe's Branch sediment yield (161.5 m/Ma). From left to right is the Black Swamp tributary, Cane Creek, Dutchman's Creek, BeeTree Creek, Cataloochee Creek, and Nantahala River.

APPENDIX C

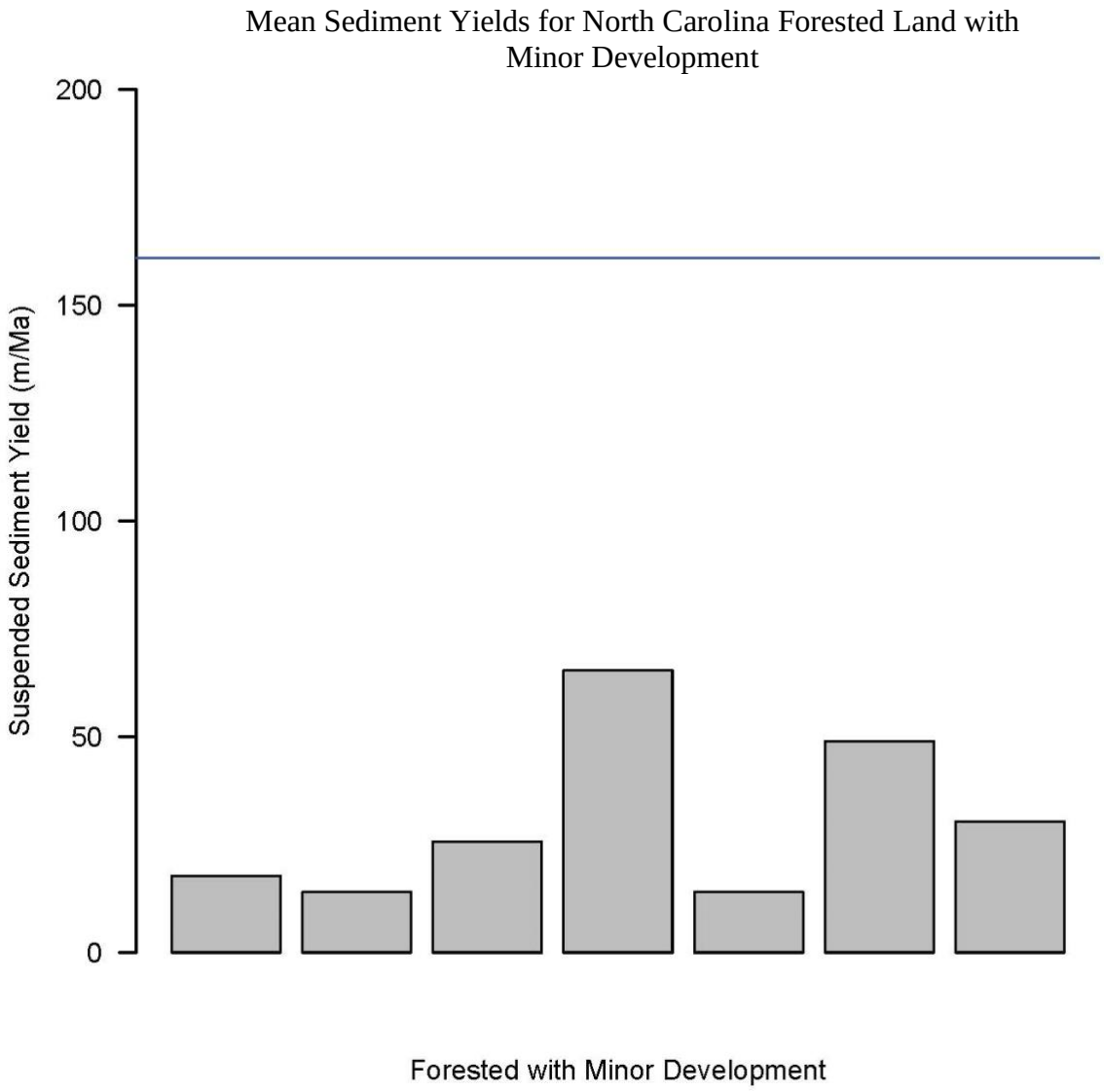

C. The bar plot shows the long-term sediment yields of North Carolina tributaries in forested regions with minor development (Simmons, 1993). The blue line represents Holcombe's Branch sediment yield (161.5 m/Ma). From left to right is the Buckhorn Creek, Flat Creek, Linville River, Jacob Fork, Davidson River, West Fork Pigeon, and the South Toe River.

APPENDIX D

Mean Sediment Yields for North Carolina Rural Agricultural/Farmland

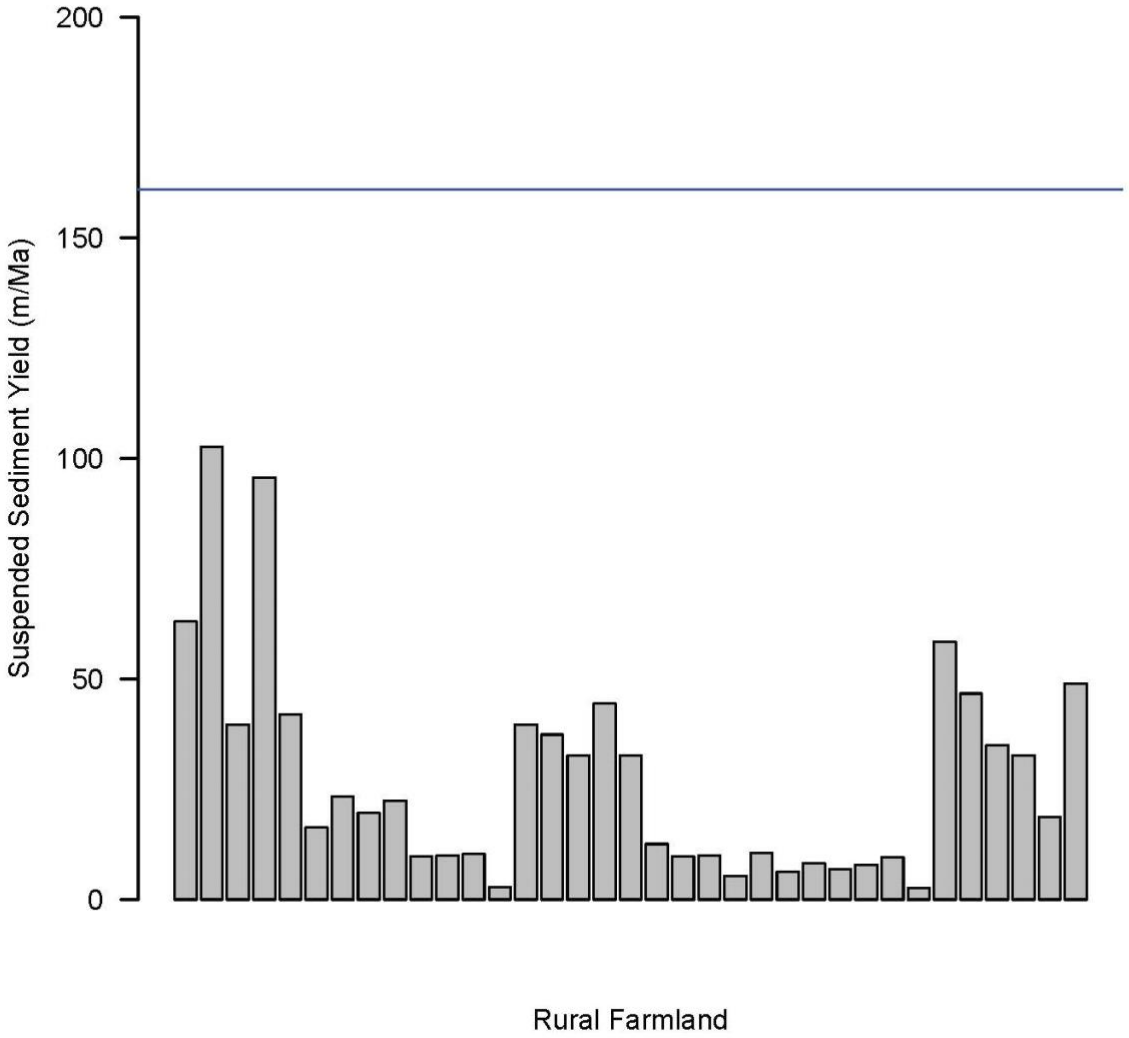

D. The bar plot shows the long-term sediment yields of North Carolina tributary's in rural agricultural/farmland regions (Simmons, 1993). The blue line represents Holcombe's Branch sediment yield (161.5 m/Ma). From left to right is the Dan River near Francisco, the Dan River near Wentworth, Hyco Creek, Double Creek, South Hyco Creek, Tar River near Tar River, Tar River near Louisburg, Cedar Creek, Swift Creek, Little Fishing Creek, Tar River near Tarboro, Chicod Creek, Durham Creek, Eno River near Hillsborough, Eno River near Durham, Little River, Flat River, Neuse River, Middle Creek, Little River near Kenly, Little River near Princeton, Bear Creek, Turner Swamp, Contentnea Creek, Little Contentnea Creek, Creeping Swamp near Calico, Creeping Swamp near Vancboro, Palmetto Swamp, Trent River near Trenton, Reedy Fork, Big Alamanace Creek, Cane Creek near Teer, Haw River, Deep River near Randleman.